Université de Bretagne Occidentale

MASTER SML

SCIENCES DE LA MER ET DU LITTORAL

MENTION

CHIMIE ET SCIENCES DU VIVANT

PARCOURS

CHIIMIE DE L'ENVIRONNEMENT MARIN

GIRARDOT Margot

160 years of environmental change in the Aulne estuary (Bay of Brest): a geochemical reconstruction of mining legacy and productivity dynamics

Mémoire de stage de Master 2

Année Universitaire 2024-2025

Structure d'accueil : Geo-Ocean, SEDISOR, LEMAR

Tuteur universitaire : WAELES Matthieu

Maîtres de stage : PENAUD Aurélie, RÉVILLON Sidonie, WAELES Matthieu, VALERO Clara

160 YEARS OF ENVIRONMENTAL CHANGE IN THE AULNE ESTUARY (BAY OF BREST): A GEOCHEMICAL RECONSTRUCTION OF MINING LEGACY AND PRODUCTIVITY DYNAMICS

Lead on ———————————————————————————

Acknowledgment

To the members of *Geo-Ocean*:

- I sincerely thank Aurélie PENAUD and Clara VALERO for offering this internship opportunity and for their time, support, numerous guidance and insightful proofreading. You gave me more than just internship supervision. Thank you for everything.

- Léonie DELALEAU and Charlotte GASNE--DESTANEVILLE for their assistance with sedimentological analyses and the preparation of diatom slides.

- Lucas BOSSEBOEUF, thank you for the numerous moments of interdisciplinary exchange as we confronted history with only geochemical data and hope. Thank you also for your research into the local press and *commodo-incommodo* archives.

- I also want to thank Jérôme GOSLIN, for our valuable discussions on the geochemical data from the Aulne estuary and river.

To the members of *SEDISOR*:

- I am truly grateful to Sidonie REVILLON and Emma DONNARD for supervising the majority of the geochemical analyses and for their patience throughout. I extend special thanks to Sidonie REVILLON for your guidance in data interpretation and your detailed proofreading.

To the members of *LEMAR*:

- I am sincerely thankful to Matthieu WAELES, for his time, numerous insights and careful proofreading. Thank you, also, for your committed pedagogical support throughout the year.

- Jill SUTTON, thank you for your expertise and for our discussions, as well as for your proofreading and consideration.

To the members of the *Pôle Spectrométrie Océna and PACHIDERM*:

- Céline LIORZOU, Marie-Laure ROUGET; Killian ANGEL, Rudolph CORVAISIER, Fabien DEWILDE and Jean-Marie MUNARON, thank you for your technical support at the *Pôle Spectrométrie Océan*, for conducting the analytical measurements (ICP-AES, ICP-MS, IR-MS), and for operating the instrumentation.

- Kevin BIHANNIC and Morgane GALLINARI, thank you for your assistance with biogenic silica measurements and for conducting analyses on the autoanalyzer.

To the members of *EPOC*:

- Sabine SCHMIDT, thank you for conducting the age model measurements and for providing its data.

And finally,

- I want to thank the members of the jury, for their attention to this work.

To everyone, thank you.

À nos moments de « Galène ».

"*Time is like a river made up of the events which happen, and a violent stream; for as soon as a thing has been seen, it is carried away, and another comes in its place, and this will be carried away too*."

- Marcus Aurelius, Meditations

Yet,

"*What we do in life, echoes in eternity*"

- Maximus, Gladiator

Table of contents

List of figures

Abbreviations

BB: Bay of Brest
bSi: Biogenic Silica

$\mathbf{C_{Org}}$: Organic C
$\mathbf{C_{Tot}}$: Total C

D50: Median grain size

EF: Enrichment Factors

IA: Interval “IA”
IB: Interval “IB”
IC: Interval “IC”
ICP-AES: Inductively Coupled Plasma-Atomic Emission Spectrometry
ICP-MS: Inductively Coupled Plasma-Mass Spectrometer
IR-MS: Isotope Ratio-Mass Spectrometer
IS02 core: PACTE-AL-IS02 core
IS04 core: PACTE-AL-IS04 core

LDS: Laser Diffraction System
LIA: Little Ice Age
LOI: Loss On Ignition

MC-ICP-MS : Multi Collector- Inductively Coupled Plasma-Mass Spectrometer

P-H: Poullaouen-Huelgoat
PCA: Principal Components Analyses
PSO: Pôle Spectrométrie Océan

RSD: Relative Standard Deviation

TOM: Total Organic Matter

WWII: World War II

XRF: X-Ray Fluorescence

1. Introduction

Coastal environments are among the most productive systems on Earth (Costanza *et al.,* 1997). Over the past two hundred centuries, their ecological sustainability has been increasingly undermined by chemical contamination linked to anthropogenic activities (Turner, 2015). Trace Metallic Elements (TMEs) exhibit high toxicity when enriched above their naturally low concentrations (<100 ppm), and are widely released through mining, smelting, agriculture, and urban or industrial effluents (Pan & Wang, 2012; IUPAC, 2014). Excessive nutrient inputs such as N and P promote eutrophication, hypoxia, and harmful algal blooms, and are used in fertilizers and manure, leading similarly to the degradation of coastal ecosystems (Richir & Gobert, 2016; Chapelle *et al.,* 2021).

Sediment cores act as natural archives for past conditions through the progressive accumulation of particulate matter (Zhou *et al*., 2019). TMEs, nutrients, and organic matter are incorporated into sediments via adsorption and settling, with their concentrations and isotopic compositions serving as measurable indicators (proxies), for past contamination intensities, sources, and ecological impacts (Chapman & Anderson, 2005; Birch *et al.,* 2015). The effect of grain size and lithological variability on concentrations are commonly reduced using Al normalized proxies (Loring, 1991). Elemental ratios such as Ti/Ca, C/N and TMEs enrichment factors additionally allow to integrate the relative influence of terrestrial *versus* marine inputs, weathering rates and redox to past environmental reconstructions and of their drivers (Meyers, 1994; Bahr *et al.,* 2005; Ishfaq *et al.,* 2013).

The Bay of Brest (BB), in western Brittany (France), is heavily stressed by anthropogenic activities (Ragueneau *et al.,* 2018). Its main tributary, the Aulne River, drains a watershed historically impacted by the Poullaouen-Huelgoat (P-H) mining complex, which produced ~20,000 tons of Pb and ~50 tons of Ag between 1760 and 1790; and which likely continues to release Pb, Cd, Zn, Ag and Hg in the Aulne River; notably through the Argent River (**Fig. 1**) (Nasri *et al.,* 2021; Daumas, 2023). Currently, the Aulne watershed is predominantly agricultural (*i.e.* 78 % of its land use), further contributing to nutrients inputs to its estuary. The spatio-temporal dynamics of these inputs remain poorly constrained, limiting effective monitoring and sustainable coastal management (Briant *et al.,* 2022).

The aim of this study is to reconstruct 160 years of environmental variability in the Aulne estuary (Bay of Brest), using two sediment cores. It focuses on geochemical proxies for major and minor elements, including oxides and biogenic proxies; and for Trace Metallic Element enrichments. A special attention is given to distinguishing terrestrial *versus* marine sources, especially the legacy Poullaouen-Huelgoat mining activity, and to exploring weathering and redox conditions. The ecological impacts of these geochemical shifts are assessed through multivariate statistical analysis.

2. Environmental context

Located in western Britanny (NW France, W Europe), the BB is a semi-enclosed bay covering 180 km^2 with an averaged depth of 8 m (~60 % of its surface < 10 m deep) and connected to the Atlantic Ocean by a strait named the 'Goulet' (**Fig.1**) (Pommepuy, 1977). The Aulne river, with a watershed of 1797 km², is responsible for most of the BB inputs of freshwaters (*i.e.* 63 % of total inputs; annual estuarine flow of ~22 m^3.s^{-1}) and sediments (*i.e.* 72 %; 7000 t.yr^{-1}) (Pommepuy, 1977; Nasri *et al.*, 2021). At its estuary, the combination of river flow with the strong semi-diurnal tidal forcing (*i.e.* 4.7 m tidal range) creates a complex hydro-sedimentary system (Pommepuy, 1977; Chauvaud *et al.*, 2000).

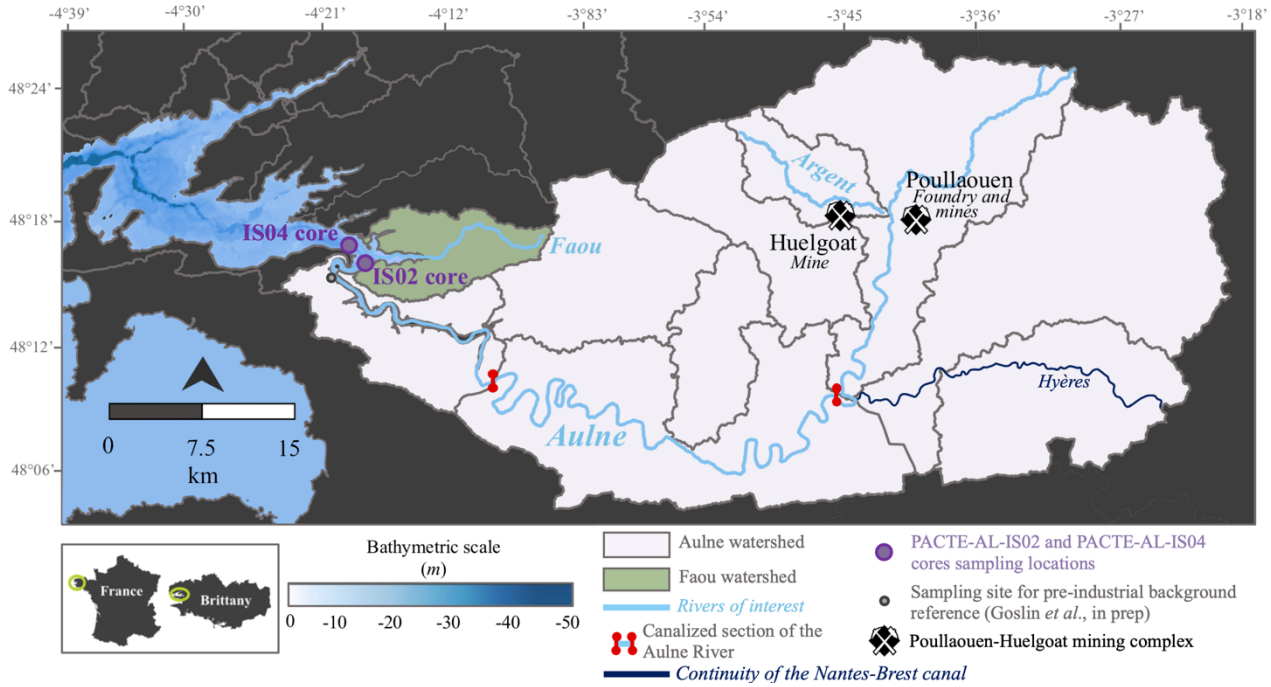

Figure 1. Map of the Bay of Brest and its southern watersheds; featuring PACTE-AL-IS02 and PACTE-AL-IS04 cores retrieving locations.

3. Materials & Methods

3.1. Study sediment cores

Two sediment cores, PACTE-AL-IS02 and PACTE-AL-IS04 (named here IS02 and IS04 respectively); were collected from the Aulne estuary during the PACTE cruise, on 3 August 2023, aboard the N/O Thalia (Ifremer), using an interface corer. IS02 core (48°17'27.3"N, 4°14'48.9"W; 5.8 m water depth) is 34 cm long and IS04 core (48°17'46.5"N, 4°15'50.88"W; 5.0 m water depth) is 54.4 cm (**Fig. 1**). Both cores were selected according to their well recorded Pb and Zn X-Ray Fluorescence (XRF) core scanner screening, apparently suited for past mining pollutions investigations (**Fig. 2**). Both cores are now stored at the *Centre de Ressources en Échantillons et Archives Marins* (CREAM; Ifremer, Brest).

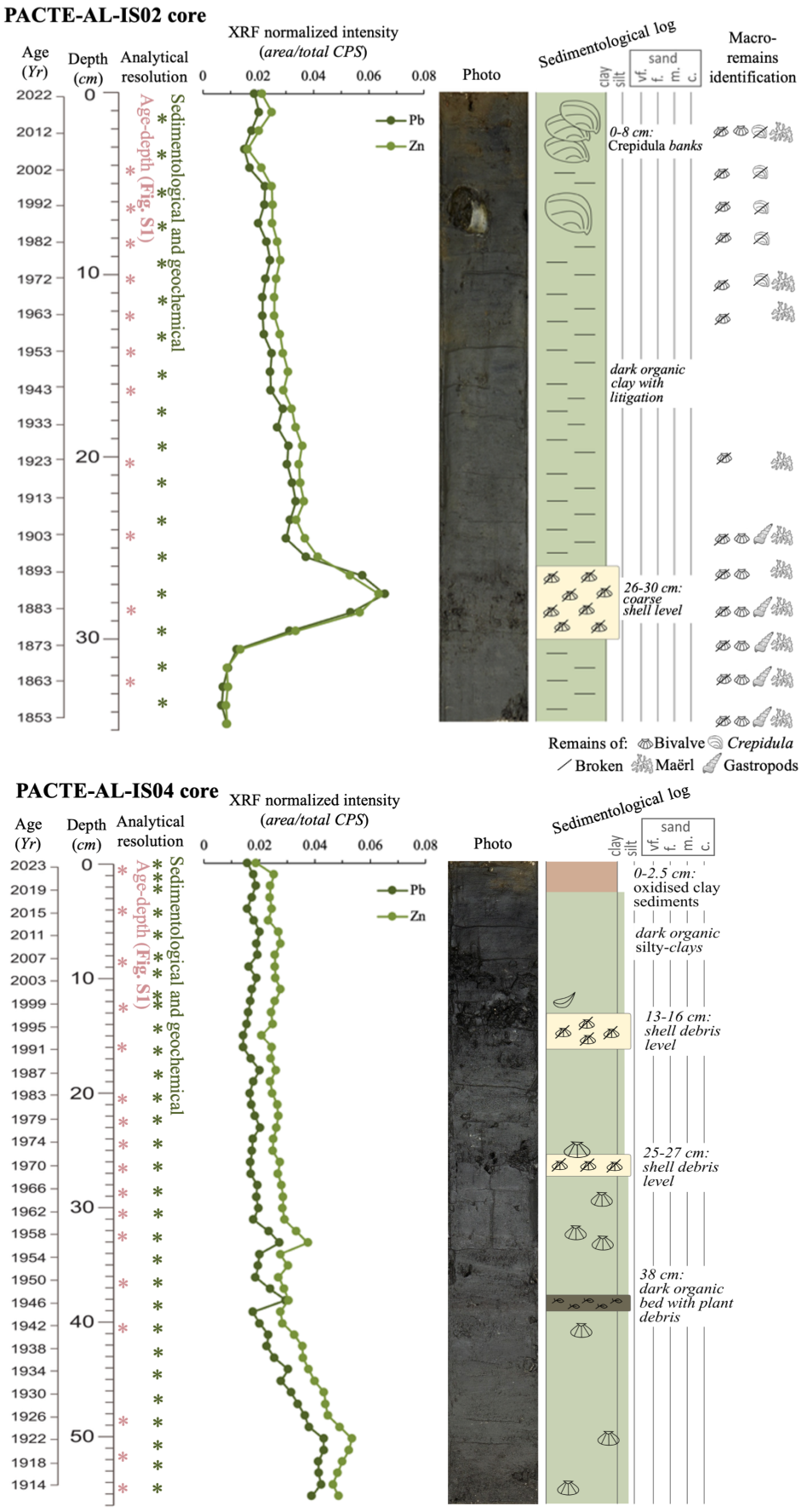

Figure 2. PACTE-AL-IS02 and PACTE-AL-IS04 cores analytical resolution, XRF profiles for Pb and Zn, photo, sedimentological log (including notable facies), and identified macro-carbonate remains (photo and sedimentological log after Valero, 2025).

3.2. Sediment cores dating

Sediments dating was established on excess ^{210}Pb ($^{210}Pb_{xs}$), ^{137}Cs, and ^{226}Ra radioactive isotopes depth activities, using a Broad Energy Germanium γ detector (BEGe; Mirion Technologies) at the EPOC laboratory (CNRS, University of Bordeaux), following Siano *et al*. (2021), with a 2 cm resolution, on 10 g of sediments powders. IS02 core covers ~160 years (1853±10.1 to 2022±0.1 AD), with a sedimentation rate of 0.2±0.01 cm. yr^{-1} (~10-year resolution); while IS04 core covers a shorter period of ~110 years (0.5±0.04 cm. yr^{-1}), with a twice higher sedimentation rate of 0.4±0.01 cm. yr^{-1} (~3-4-year resolution) (**Fig. S1**).

3.3. Sedimentological analysis

Grain-size distributions were measured using a Laser Diffraction System (LDS; Mastersizer 2000, Malvern panalytical®) at the IUEM (Plouzané, France), on 1 g of decarbonated sediment powders (dissolved in 37 % HCl). Median grain size (D50) and volumetric fractions were obtained using GRADISTAT v8.0 software (Blott & Pye, 2001). The bio-indicator macro-carbonate remains of IS02 core were additionally identified after sieving (>150 µm), using a binocular.

3.4. Geochemical analysis

3.4.1. Major and minor elements

3.4.1.a Proxies for the mineralogical composition

The concentrations (%) of major and minor oxides were measured using an Inductively Coupled Plasma-Atomic Emission Spectrometer (ICP-AES; Jobin-Yvon Ultima 2, Horiba®), at the *Pôle Spectrométrie Océan* (PSO; Plouzané, France) following Cotten *et al.* (1995). Prior to measurements, 250 mg of sediment powders were digested in Teflon® beakers (Savillex®), using 32 % HCl (3 mL) + 65 % HNO_3 (1 mL) + 40 % HF (3 mL) on a hot plate at 90°C for a week. A 20 $g.L^{-1}$ $H_3BO_3^-$ (93 mL) solution was then added to neutralize HF, break down SiF_6^{2-} and to serve as an internal standard. Calibrations were made using international standards (AC-E, BELC, CB2, CB15, CB18, JB-2 and JG-2), prepared in the same batch. Analytical accuracies and precisions were determined using external standards (ME and WS-E; Relative Standard Deviations - RSD were ≤ 3 % for SiO_2 and ≤ 5 % for other elements). Oxide recoveries ranged between ~94 and ~101 % (**Tab. S1**). Elemental concentrations (%) were then normalized to Al and Ti/Ca ratio were calculated.

3.4.1.b. Proxies for the biogenic productivity

The concentrations of Total C (C_{Tot}, %) and N (N, %), and their stable isotope ratios ($^{13}C/^{12}C$ and $^{15}N/^{14}N$) were measured using an Elemental Analyzer (EA; EA-Flash 2000™, Thermo Scientific™) coupled to a gas Isotope Ratio-Mass Spectrometer (IR-MS; DELTA V Plus™, Thermo Scientific™) at the *PSO*, on 5 mg of sediment powders. Ratios were expressed as δ ($\delta^{13}C$ and $\delta^{15}N$; ‰), measuring the deviation from the ratios of a standard (Vienna Peedee Belemnite for C; atmospheric N^2 for N)

(*cf.* **Eq. 1**). Analytical precisions were determined using an internal standard (98 % Acetanilide, Thermo Scientific Chemicals™; RSD were < 0.8 % for C, < 0.1 % for N, and < 0.15 % for $\delta^{13}C$ and $\delta^{15}N$). C_{Tot}/N ratio were then derived from C_{Tot} and N.

$$\delta X = \frac{R_{Sample} - R_{Standard}}{R_{Standard}} \times 1000 \quad \textbf{(1)}$$

Where X is $^{13}C_{Tot}$ or ^{15}N, and R_{Sample} and $R_{Standard}$ the respective $\delta^{13}C$ or $\delta^{15}N$ of samples and standards.

The concentrations of Total Organic Matter (TOM, %), and $CaCO_3$ ($CaCO_3$, %), were measured using a muffle furnace following Heiri *et al.* (2001), on 1 g of sediments powders. The concentrations of biogenic Silica (bSi, %) were measured following the molybdenum blue method (Aminot & Kerouel, 2007), using an autoanalyzer (AA3 HR Autoanalyzer®, SEAL Analytical®), on 50 mg of sediments powders. Prior to measurements, bSi was extracted using 0.5 M NaOH, following the sequential extraction method of DeMaster (1981) for 8 h (RSD ~10 %).

3.4.2. Trace elements: Proxies for TMEs enrichment and sources, and of redox conditions

The concentrations of a selection of Trace Metallic Elements (*i.e.* Ag, Cd, Co, Cr, Cu, Hg, Mo, Ni, Pb, U, V, Sb and Zn; ppm) were measured using a High Resolution-Inductively Coupled Plasma-Mass Spectrometer (HR-ICP-MS; Element XR™, Thermo Scientific™) at the *PSO*, following Charles *et al.* (2021). Prior to measurements, in clean laboratory, 100 mg of sediments powders were digested in screw top Teflon® beakers (Savillex®), using ultrapure Quartex 14 N HF (2 ml) + 14.4 N HNO_3 (1 ml) (90°C for 48h). Samples were evaporated (to dryness); and trace elements dissolved using ultrapure Quartex 14.4 N HNO_3 (1 mL) + 10 N HCl (3 mL) (90°C for 48 h). Samples were then evaporated and diluted as mother solutions using ultrapure Quartex 6 N HCl (10 mL). A few hours before measurements, 400 µL of mother solutions were evaporated and diluted 25 times using a 0.4 N HNO_3 solution containing six drops of 32 N HF. Calibrations were made using BHVO-2 solutions prepared in the same batches. Sample concentrations were determined using Tm as an internal standard (30 ng of Tm per mg of sample), and using BHVO-2 solutions as a bracketing standard, following Barrat *et al.* (2012). Analytical accuracies and precisions were determined using international standards (BCR-2, JG-2 and JSd-3; RSD were ≤ 5%). Enrichment Factors (EFs) were calculated using the pre-industrial (1750) background of the Aulne river banks, near its estuary (*cf.* **Eq. 2**) (**Fig. 1**) (Goslin *et al.*, in prep).

$$EF_X = \frac{\left(\frac{X}{Al}\right)_{Sample}}{\left(\frac{X}{Al}\right)_{Pre-industrial\ geochemical\ background}} \quad \textbf{(2)}$$

Where X and Al are respectively the TMEs and Al concentrations.

Pb radiogenic isotope compositions were measured using a Multi Collector-Inductively Coupled Plasma-Mass Spectrometer (MC-ICP-MS; Neptune™, Thermo Scientific™) at the *PSO*, following Gale (1996). Prior to measurements, Pb was isolated from 3mL of mother solutions, using 0.1 mL of ion exchange resins (Sr spec™, TrisKem®). Prior to loading, solutions were evaporated and diluted using 2 N HCl (1 mL). Resins were rinsed using 6 N HCl and Mili-Q water; and then conditioned using 2 N HCl (3 mL). Samples were loaded; Pb stripped using two portions of 2 N HCl (1 and 2 mL respectively); and recovered using three portions of 6 N HCl (1 mL each). Pb isolates were then evaporated, dissolved using 1 N HNO_3 (0.5 mL), and re-evaporated to be diluted using 2.5 HNO_3 specific with sample specific dilution factors to standardize concentrations. Mass fractionation and instrumental bias were corrected using Tl as a dopant, following White *et al.* (2000); with NIST SRM981 Pb as a bracketing standard every two samples. Repeatability, based on 26 replicates of SRM981, were <0.003 for $^{206}Pb/^{204}Pb$, <0.002 for $^{207}Pb/^{204}Pb$ and <0.006 for $^{208}Pb/^{204}Pb$.

3.4.2. Representation of data and statistical analysis

IS04 core proxies were smoothed using 2-3 points moving averages to match IS02 core's resolution (10 years). Supplementary quantitative analyses were made using R software (R Core Team, 2025). Intra-core proxy relationships were assessed using Principal Components Analyses (PCA) with the *prcomp()* function (data scaling and normalization).

3.5. Diatom analysis

Diatom assemblages of IS02 core were determined in duplicate, identifying at least 200 benthic frustules (species level whenever possible), using a photonic microscope (Leica DM2500®, Leica Microsystems GmbH) with a 100x oil immersion objective lens and supplied with a differential interference contrast. Slides were mounted on 1.5 g of sediment powders following Crosta *et al.,* (2020), frustules counted following Crosta and Koç (2007), and identifications based on Paulmier (1997); Park *et al.* (2012); Kihara *et al.* (2015); Siqueiros Beltrones *et al.* (2016) and Siqueiros Beltrones *et al*. (2021). Data were preliminary are hence not presented in the results section. More details about the methodology and data are provided in the Supporting information.

4. Results

4.1. Multi-proxy framing

For comparisons between IS02 and IS04 cores, studied at lower and higher resolutions respectively, values are presented as raw data while patterns are described as moving averages. Despite these differences, both cores exhibit similar temporal trends. IS02 core has distinct proxy values, characterized by a lower variability than IS04 core patterns (**Fig. 3**; **Fig. S2**). Most signals are

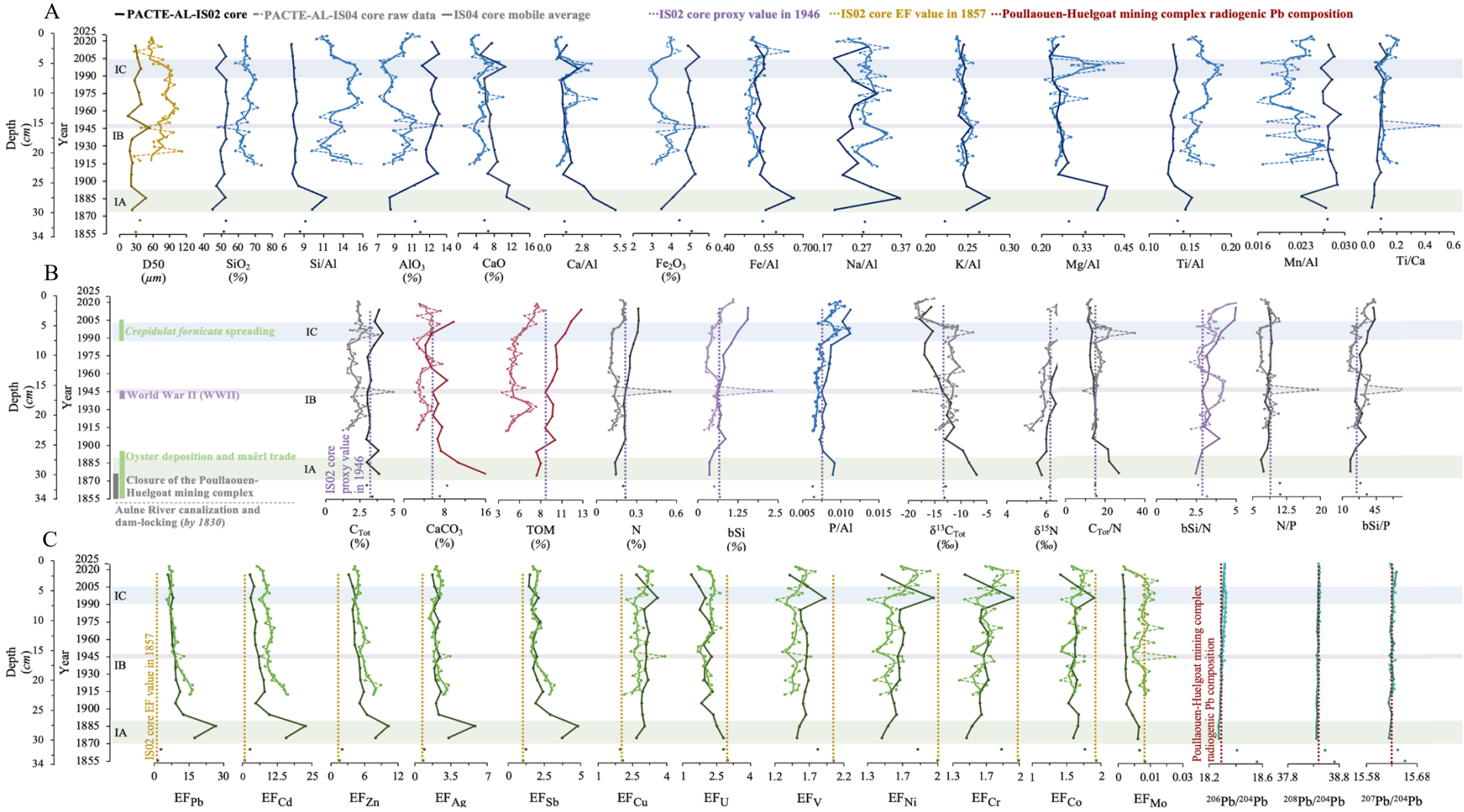

Figure 3. PACTE-AL-IS02 and PACTE-AL-IS04 cores multi-proxy data for (**A**) grain sizes (brown curves, LDS data) and mineralogical composition (blue curves, ICP-AES data); (**B**) biogenic productivity (IR-MS data, grey curves; sequential LOI data, red curves; bSi extraction, lavender curves), featuring chronological markers of key anthropological and ecological events in the Bay of Brest and the Aulne River watershed; (**C**) Trace metallic elements Enrichments Factors (EF) and sources, featuring redox sensitive elements (ICP-MS data, green curves; MC-ICP-MS data, teal curves). **IA**, **IB** and **IC** stand respectively for Intervals "IA", "IB" and "IC". The two lower curves lines were not traced due to chronological uncertainties *(5.1.2.b)*.

first disrupted (peaking or troughing) between 1876 and 1916 (Interval A; "IA" in **Fig. 3**). From 1915 to 1996, patterns are either temporally stable for most mineralogical composition proxies, while slightly increasing for most biogenic productivity proxies, or declining for some TME enrichment proxies. Additional disruptions occur around 1946 in IS04 core for biogenic proxies ("IB" in **Fig. 3**); and around 1996-2006 in both cores for some mineralogical proxies ("IC" in **Fig. 3**). These intervals occur within observed lithological facies (**Fig. 2**; **Fig. 3**; **Fig. S2**).

4.2. Grain-size and proxies for the mineralogical composition

Core IS02 consists of finer, silty-clayey sediment (mean D50 of ~29 µm; low variability), in contrast to the coarser very fine sandy sediment of IS04 core (mean D50 of ~75.5 µm; high variability) (**Fig. 3A**). Core IS02 displays two bioclasts-rich intervals; 1876-1896 (maërl debris, bivalve and gastropod shells; "IA") and 1996-2016 (*Crepidula* and bivalve shells, "IC"). Core IS04 also reveals two bioclast intervals; 1970-1974 (Bivalve shells) and 1995-1999 (*Crepidula* shells). In both cores, SiO_2 and Al_2O_3 dominate with lower SiO_2 values in IS02 core (~50 %) than in IS04 core (~65 %); and Al_2O_3 displaying the opposite trend (IS02 core value of ~14.5 %; IS04 core value of ~8.5%). CaO (IS02 ~8 %; IS04 core ~5 %) and Fe_2O_3 (IS02 ~5.7 %; IS04 core ~4 %) follow in abundance while other oxides are <1% (**Fig. S2A**). During the interval A, referred to as "IA", most oxide concentrations and Ti/Ca trough concomitantly while CaO rise from 4.86 % in 1865 to 9.9 % in 1875. In contrast, all Al-normalized proxies apex. The interval "IB" is characterized by weaker disruptions for most normalized signals; while the interval "IC" affects notably Ca-, Mg-, Mn/Al and Ti/Ca. In both cores, CaO is generally anti-correlated to SiO_2 and so is Si/Al to Al (**Fig. 4**; **Fig. S3**; **Fig. S4**). Environmental pressures likely altered the mineral matrix, affecting biogenic and TME proxy signals.

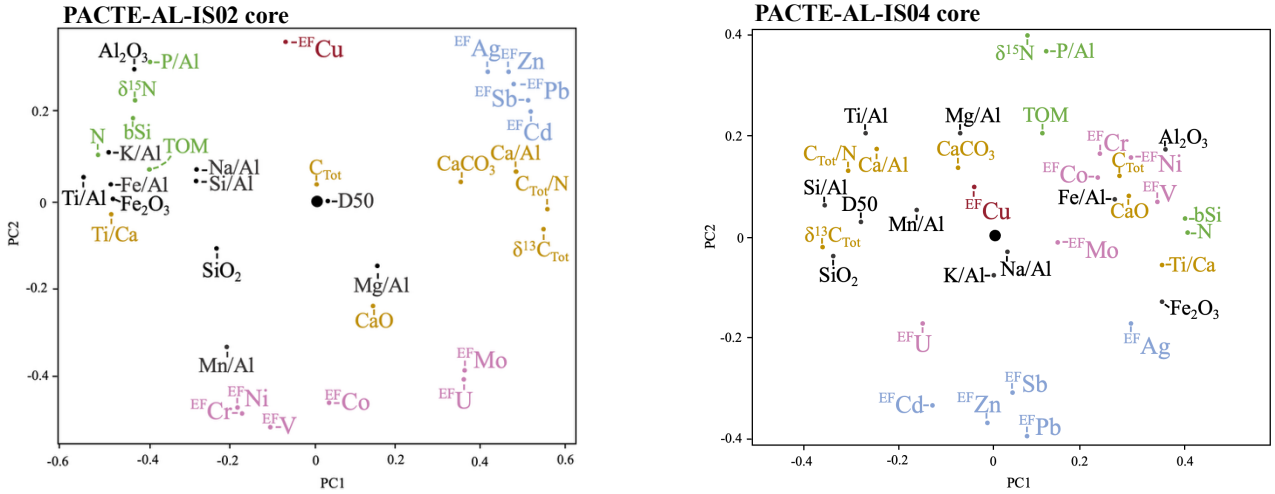

Figure 4. PACTE-AL-IS02 and PACTE-AL-IS04 cores Principal Component Analysis (PCA) on proxy data. Analysis includes the proxies most relevant for biogenic productivity (green); assessing the pollution from the Poullaouen-Huelgoat mining complex (blue); weathering and redox conditions (pink); and proxies numerically influenced by carbonate shell banks (gold). For PCA on temporally clustered sequences, see **Fig. S3**; **Fig. S4**.

4.3. Proxies for biogenic productivity

Core IS02 displays higher average concentrations of proxies for biogenic productivity than core IS04 (C_{Tot} ~3.3 *vs*. 2.32 %; $CaCO_3$ ~7.5 vs. 2.3 %; TOM ~9.5 *vs*. 5.5%; N ~0.2 *vs*. 0.16 %; bSi ~0.8 *vs*. 0.55 % and P/Al ~0.08 *vs*. 0.07) despite similar $\delta^{13}C$ and $\delta^{15}N$ values (~-13.3 and ~6.20 ‰ respectively) (**Fig. 3B**; **Fig. 4**). In both cores, C_{Tot}, N, P/Al, bSi, $\delta^{15}N$ values exhibit similar patterns, opposite to C_{Tot}/N and $\delta^{13}C_{Tot}$. During "IA", C_{Tot}, N, P/Al, bSi, $\delta^{15}N$ values reach *minima*, then increase post-1946 (most notably in IS02 core) up to two folds by 2016/2023. Ratios such as C_{Tot}/N, bSi/N, N/P and bSi/P follow more closely their numerator trends in IS02 core than in IS04 core. Hence, both cores record similar biogeochemical processes, yet with higher intensity in IS02 core.

4.4. Proxies for TMEs enrichments and sources, and of redox conditions

Selected TMEs exhibit near-baseline enrichment factors (EFs) in 1856 (0.8–2), except Mo (~0.01) and Hg (below quantification limits). EF patterns diverge afterward into distinct yet groupable trajectories (**Fig. 3C**; **Fig. 4**). In both cores, Pb, Cd, Zn, Ag, and Sb exhibit apexing EFs during Interval A, reaching maxima in 1886 (Sb ~4.8 to Pb ~26.5). However, corresponding absolute concentrations (0.41–650 ppm) are not consistently the highest among TMEs (*i.e*., Ag, Cd, and Sb concentrations remain lower than those of Cu) (**Fig. S2C**). Post-"IA", EFs decline toward 2016/2023 period, yet remain at least twice their 1856 levels (*e.g*., Pb 5.1; Cd 3.9; Zn 3.7; Ag 1.9; Sb 1.6; based on somital averages). In addition, EF values for Pb, Cd, Zn, Ag and Sb are significantly correlated with $CaCO_3$, (**Fig. 4; Fig. S3C**). Cu values mirror the early rise of Pb, Cd, Zn, Ag, and Sb, reaching EF ~3 in 1886, but diverges subsequently, remaining stable except for a peak during "IC" in IS02 (EF ~4). U, V, Ni, Cr, Co, and Mo display similar EF patterns within each core, but differ between cores. IS02 core signals decline after "IA" and remain stable, aside from a minor peak during "IC" (V, Ni, Cr and Co, akin to Cu). Conversely, IS04 core EFs fluctuate without clear trends. Mo exhibits the most pronounced inter-core differences (IS02 core 0.01-0.02; IS04 core 0.002-0.02). In contrast, Ni, Cr, and V display similar ranges across cores (1.2-2.05). U, V, Ni, Cr, Co and Mo show no correlation with specific oxide phases.

Lead isotope ratios ($^{206}Pb/^{204}Pb$, $^{207}Pb/^{204}Pb$ and $^{208}Pb/^{204}Pb$) (**Fig. 3C**) exhibit similar trends across both cores, decreasing from their 1956 maxima (18.56, 15.65 and 38.70; IS02 core data) to their 1876 minima (18.27, 15.62 and 38.35, IS02 core data) followed by a gradual rise by 2016/2023 period (to 18.31, 15.63 and 38.41, IS04 core data). Hence, several TMEs display aligned EF patterns within and between cores (*e.g*., Pb, Cd, Zn, Ag, Sb; U, V, Ni, Cr, Co, Mo), suggesting shared sources, geochemical behaviour, or sediment binding phases, while Cu may be introduced by two distinct and successive sources.

5. Discussion

5.1. Proxies for the mineralogical composition

Most major and minor oxide concentrations align with typical estuarine sediment signatures, except for elevated CaO (**Fig. 3A**; **Fig. S2A**) (Negrel, 1997; Whitemore *et al.,* 2004; Ip *et al*., 2007; Liu *et al.,* 2012; Yano *et al*., 2020). During Intervals "IA" and "IC", the co-occurrence of CaO peaks with troughs in other oxides and their inverse correlations suggest dilution by Ca-rich inputs (Yano *et al*., 2020). The fine and stable grain-size distribution of IS02 core compared to IS04 core suggests deposition in a lower energy environment (**Fig. 1**) (Orton & Reading, 1993). In contrast, the coarser and more variable grain-size in IS04 core despite a higher sedimentation rate, imply a stronger susceptibility to tidal remobilization (Orton & Reading, 1993). Differences in absolute geochemical proxy values between the two cores are likely driven by grain-size contrast, resulting in distinct mineral compositions (Pettijohn *et al.,* 2012). This hypothesis is supported by Al-normalization reducing inter-core differences (**Fig. 3**; **Fig. S2A**; **Fig. S2C**). Despite greater variability in IS04 core, the consistent temporal patterns observed in both cores support a common regional forcing. IS02 core, with finer sediments, lower variability, and longer chronological coverage, is thus better suited for paleoenvironmental reconstruction.

5.2. Proxies for TMEs enrichments and sources, and of redox conditions

5.2.1. Proxies for the pollution from the Poullaouen-Huelgoat mining complex

5.2.1.a. Framing of the proxies for the pollution from the Poullaouen-Huelgoat mining complex

The concentrations and EF of Pb, Cd, Zn, Ag, Sb and Cu from 1946 to 2016/2023, and the Pb radiogenic isotope composition align with modern values of the Aulne estuarine sediments and riverine waters (**Fig. 3C**; **Fig. S2C**). These elements are likely co-originating mainly from the Poullaouen-Huelgoat mining complex through the continuous leaching of its remaining ores and tailings (**Fig. 1**; **Fig.4**) (Chiffoleau, 2017; Briant *et al*., 2022; Le Goff *et al*., 2023). The primary output of the P-H complex was indeed galena (PbS; Pb ~87 %; Ag ~5 ppm), primarily associated with sphalerite ([Zn, Fe]S; Cd being a substitute for Zn), and chalcopyrite ($CuFeS_2$) (Chauris & Marcoux, 1994). This hypothesis is supported by their concentrations and EF values falling in the typical elemental ratios associated with Pb-Zn mining polluted area; and by the Pb radiogenic isotope compositions exhibited by both cores from 1886 to 2023, which correspond to the one displayed by the Poullaouen-Huelgoat mining complex ($^{206}Pb/^{204}Pb$ ~18.3) (**Fig. 3C**) (Chauris & Marcaux, 1994; Anju & Banerjee, 2011; Zhu *et al*., 2018; Sun *et al*., 2021; Zhang *et al*., 2023). Maximal EF for Pb, Cd, Zn, Ag and Sb in 1886 correspond to very high enrichments (Pb, Cd; 20-40); significant enrichments (Zn, Ag; 5-20) and to moderate enrichments (Sb; 2-5), while modern pollutions are moderate (EF of 2-5) (Sutherland, 2000).

The EF signals of Pb, Cd, Zn, Ag and Sb are correlated to $CaCO_3$, first suggesting their sorption by this phase. Pb, Cd and Zn exhibit strong affinities towards the carbonaceous phase under neutral to alkaline conditions. The assumed role of $CaCO_3$ in their enrichment however remains unclear; as previous studies report significant enrichment while other none, even in mining-impacted sediments with $CaCO_3$ content exceeding 50 %) (Serpaud *et al.,* 1994; Šurija & Branica, 1995; Pascaud *et al*., 2015). The dilution effect of the normalizer (Al) caused by $CaCO_3$ nevertheless appears to poorly magnify EF values, for Pb, Cd, Zn, Ag and Sb are not anticorrelated to Al_2O_3 (**Fig. 4**; **Fig.S3A**).

5.2.1.b. Histories of the proxies for the pollution from the Poullaouen-Huelgoat mining complex

In 1857, low enrichment factors for Pb, Cd, Zn, Ag, Sb, and Cu (EF < 2) and Pb isotopic compositions ($^{206}Pb/^{204}Pb$ > 18.5) match geogenic, pre-industrial backgrounds (Sutherland, 2000; (Elbaz-Poulichet *et al*., 1986) (**Fig.3**). This is inconsistent with severe contaminations from the Poullaouen-Huelgoat (P-H) mining complex during its peak activity, from 1750 to 1790; which would likely have induced persisting pollution given their post-1886 patterns. The lack of contamination in 1857 suggests the presence of a stratigraphic hiatus in IS02 core which may have suppressed records of past mining activities. This is supported by a significant reduction in sedimentation rates (from 0.35 to 0.25 $cm \cdot yr^{-1}$) between 30 and 28 cm, and may be caused by high-energy erosive events during the Little Ice Age (LIA, 1400-1850) or by the deposition of carbonate-rich debris (*e.g.,* oyster shells and maërl) in the 19th century (Van Vliet-Lanoë *et al*., 2014) (see **5.3.2**) (**Fig. 5**). A ^{14}C-dated oyster shell from 1014 AD, located just below the equivalent interval in the twin core of PACTE-AL-IS04 core (*i.e*., PACTE-AL-KS04 core), reinforces this interpretation (**Fig. S5**). This potential hiatus may be further constrained through ^{14}C dating of carbonate macro-remains (*e.g*., *Bittium reticulatum* shells) and TMEs quantification in carbonate-bound fractions (Frontalini & Coccioni, 2008) (**Fig. 5**).

Furthermore, EF maxima around 1886 appear delayed relative to the closure of the mining complex (1866-1870). This offset may result from secondary inputs such as tailings collapse, reuse, hydrochemical remobilization, or the canalization and dam-locking of the Aulne River by 1850 (**Fig. 1**) (Sedláček *et al*., 2013; Frémion *et al*., 2016; Thienpont *et al*., 2016). Age model uncertainties, may contribute, as $^{210}Pb_{xs}$ activities below 20.5 cm in IS02 core (1923) are insufficient (3 ± 7 $Bq \cdot kg^{-1}$) to constrain an accurate stratigraphy (**Fig. 5**). In addition, the correlation between $CaCO_3$ and TMEs may point towards accumulation in maërl, which grows slower (1 $mm.yr^{-1}$) than the sedimentation rate (0.2 $cm \cdot yr^{-1}$) (Grall & Hall-Spencer, 2003). The presence of a potential hiatus suggests that the apparent EF apex may be relatively low compared to peak activities of the P-H complex (1755-1770); and may not reflect a sharp increase, but rather high temporal variability in TMEs inputs.

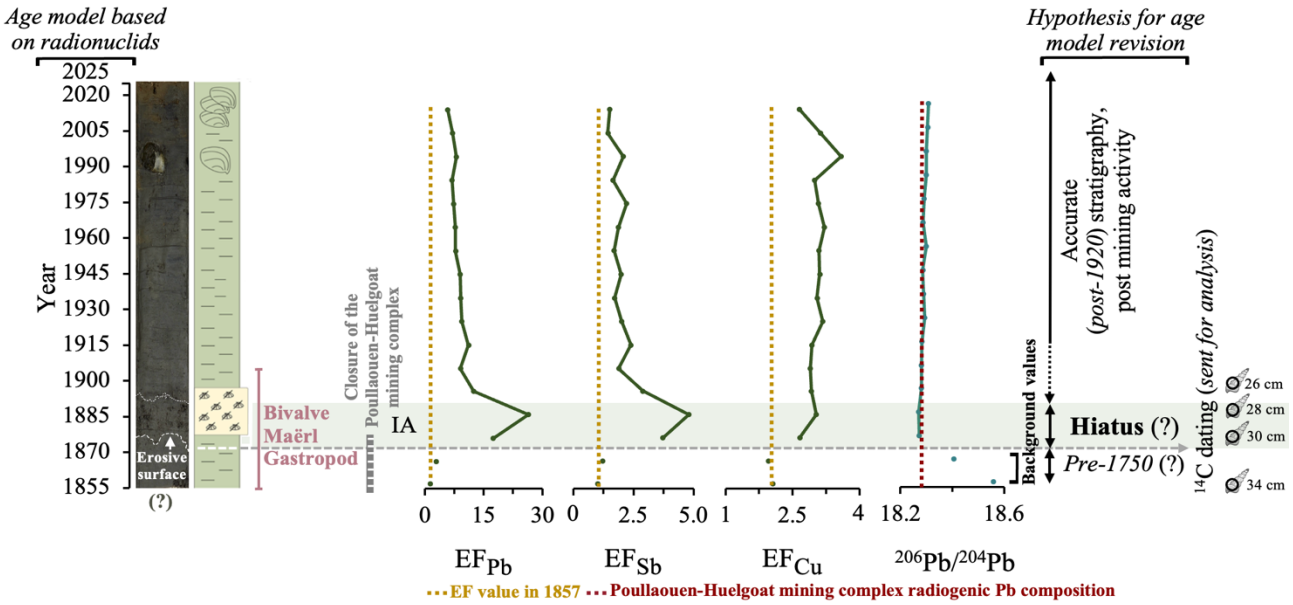

Figure 5. PACTE-AL-IS02 core integrated summary of the proxies for Trace Metallic Elements enrichments and sources; highlighting key sedimentological features, potential environmental drivers, and ongoing analysis.

The progressive decline in EF for Pb, Cd, Zn, Ag, and Sb post-1886 likely reflects the closure of the P-H complex and the subsequent weathering of residual ores and tailings, leading to a persistent and diffuse contamination with limited regulation (Anju & Banerjee, 2011). Cu, however, diverges as its EF increase post-1986 (from ~3 to ~4 by 2016-2023). Post-mining, Cu contamination likely stems from livestock agriculture as since the late 19th century, Cu has been widely used in pig and poultry feed, manures spreading (pigs excrete ~1,000 mg Cu.kg^{-1} dry matter, with ~15 Mt of slurry produced annually in the region), and fungicides (*e.g.*, $CuSO_4$, Bordeaux mixture) (Flatrès, 1963; Jones & Jarvis, 1981; Recensement Agricole, 2010; Guo *et al.,* 2018; Gourlez *et al.,* 2022). In addition, current Cu concentrations in the Aulne River match agricultural baselines, supporting sustained rural inputs (Briant *et al.,* 2022). Thus, while the pollution from the P-H complex is historical, persistent and due to a local source for Pb, Cd, Zn, Ag and Sb; the Cu contamination would reflect a dual-phase source: early mining and ongoing agricultural diffuse applications.

5.2.2. Proxies for weathering and redox conditions: V, Ni, Cr; U, Co, and Mo

Post-1857, V, Ni, and Cr display low enrichment factors (<2) (Sutherland, 2000) (**Fig. 3C**). Their synchronous decline by 1876 may reflect the fading influence of coal combustion from the declining Poullaouen foundry. This is however inconsistent with their relative abundance in coal, and with an age model revision (Reynolds, 1948). Their correlation with Al_2O_3 from 1857 to 1896 nevertheless suggests EF reductions due to lowered terrestrial inputs (despite their low abundance in the Britanny granitic lithogeny), though the chronological placement of this interval remains uncertain (**Fig. 5**; **Fig. S3**) (Liang *et al*., 2000).

Concurrently, U, Co, and Mo display similar declines, suggesting an overprint by redox processes (**Fig. 3C**; **Fig. 4**) (Tribovillard *et al*., 2006). The presence of red-orange micro-nodules, likely Fe/Mn oxy-hydroxides (*e.g*. goethite or ferrihydrite), supports this; pointing towards oxidative precipitation at redox transitions (Morford & Emerson, 1999). This is supported by V, Ni, and Cr being anti-correlated to Fe/Al (Algeo & Liu, 2020). In addition, their stronger depletion compared to U, Co, and Mo during Interval "IA" may result from $CaCO_3$-driven dilution, as suggested by their inverse relationship. Such redox transition may stem from the sharp reduction in sedimentation rates, likely to be associated to lowered organic matter inputs and oxygen demand for its remineralization, resulting in enhanced oxidation (Calvert & Pedersen, 1992). Supporting this, EF_{Mo} are higher in IS04 core, (displaying a faster sedimentation), further highlighting Mo sensitivity to redox conditions. EF_{Mo}, however displaying depleted values in both cores (< 1), are likely due a local site effect. In addition, normalized REE patterns yet show no Ce or Eu anomalies, implying redox transitions may have been too subtle to significantly fractionate REEs (**Fig. S6**; **Fig. S7**) (Tribovillard *et al*., 2013). Moreover, the lack of correlation between weathering-, redox- and biogenic proxies implies that productivity was neither driven directly natural terrestrial inputs, nor submitted to anoxic pressures; but rather enhanced by the higher availability of anthropogenic nutrients post-1946.

The distinct increase in EF of Cu, V, Ni, Cr and Co around 1996 possibly aligns with a bioremediation experiment focusing on crude oil degradation through fertilizer addition (**Fig. 3C**; **Fig. S2C**) (Oudot *et al.,* 1995). The signal of this event, rich in petrogenic metals (excluding Co), would differ from earlier anthropogenic signatures being intentional and experimental. The trends of U, V, Ni, Cr, Co, and Mo hence may illustrate a complex interplay between $CaCO_3$-driven dilution, hydrological shifts, redox dynamics, and later remediation experiments; altogether likely shaping the geochemical dynamics of the Aulne estuary.

5.3. Proxies for biogenic productivity

5.3.1. Framing of the proxies for the biogenic productivity

Both cores display similar biogenic proxy patterns, yet differing signal intensities; likely due to the coarser grain size of IS04 core inducing dilution and enhancing remineralisation (**Fig. 3B**) (Bergamaschi *et al*., 1997). This is additionally supported by proxy convergences when grain sizes align. Modern values are consistent with the Aulne estuary data from prior studies, and indicate moderate productivity; except for unusually high $CaCO_3$ (Sholkovitz & Price, 1980; Raimonet *et al.*, 2013, 2023; Dan *et al*., 2021). The co-variation of TOM, N, P/Al, bSi and $\delta^{15}N$ suggests a common productivity driven source, with minimal post-depositional alteration (**Fig. 3B**; **Fig. 4**). This hypothesis is consistent with the alignment of bSi/N, bSi/P and bSi signals, which support diatom

dominated signals in the BB for most part of the year (Siebert *et al*., 2024). The stable N/P ratio in IS02 likely reflects finer grain-size, enhancing P retention, whereas the higher and more variable N/P in IS04 core may result from P losses in coarser sediments, rather than distinct nutrients dynamics (Stone *et al*., 1995). The strong correlation between $CaCO_3$, C_{Tot}, $\delta^{13}C_{Tot}$ indicate carbonate dominance, limiting the use of $\delta^{13}C_{Tot}$ and C_{Tot}/N to distinguish the sources for the organic matter. Similar trends in $CaCO_3$, CaO and Ca/Al support this, with lower CaO compared to $CaCO_3$ likely due to carbonate volatilization during ICP-AES measurements, which is supported by high Loss On Ignition (LOI) in $CaCO_3$-rich intervals (Lechler *et al*., 1987; Murray *et al.,* 2000).

5.3.2. Histories of the proxies for the biogenic productivity

Interval “IA” displays sharp rises in $CaCO_3$, likely from episodic inputs of biogenic calcareous material. These may result from historical oyster shell deposition to support declining *Pecten maximus* stocks in the mid 19th century; and/or ballast dumping of maërl and coquina linked to the soil amendment trade in the Faou River (**Fig. 1**; **Fig. 2**; **Fig. 3**) (Bosseboeuf, 2024). Alternatively, intensified remobilization of carbonate beds during LIA storms, or the natural presence of an unrecorded maërl bank (supported by its high biodiversity and the presence of intact small shells) may explain these inputs (**Fig. 2**) (Van Vliet-Lanoë *et al*., 2014). Elevated Ca during “IA " limit the reliability of Ti/Ca as a proxy for marine *versus* terrestrial inputs, and also likely dilute the concentrations of other proxies. This is supported by elevated P/Al, likely linked to declining Al_2O_3. However, the lack of anti-correlation between $CaCO_3$ and other biogenic proxies during “IA” suggest real ecological shifts, as supported by the concurrent $\delta^{15}N$ drop (unaffected by dilution) (**Fig. S3**).

Decreases in the concentrations of the biogenic proxies may hence represent a higher dissolution due to higher grain size, or lowered *in-situ* productivity, likely due to increased TME concentration (Bergamaschi et al., 1997) (**Fig. 3**). This may be supported by lighter $\delta^{15}N$ values, either reflecting increased terrestrial organic matter input or reduced marine productivity (Kendall & McDonnell, 2012). Suppressed denitrification under increasingly oxic conditions, (indicated by declining EF_{Mo}; see **5.2.2**) and elevated Zn, may also have further lowered $\delta^{15}N$ (Jensen *et al*., 1994; Magalhães *et al*., 2007). Yet, concurrently increased foraminifera abundance and diversity int the Aulne estuary are inconsistent with a scenario of decreased productivity (**Fig. 6**) (Tilman, 1982; Chaumartin, 2025). Foraminifera may nevertheless have benefited from the carbonate debris providing favourable microhabitats. Interval “IA” thus reflects both carbonate-driven dilution and real environmental shifts, followed by a period of progressively rejuvenated productivity.

Interval "IB”, which is recorded only in IS04 core, reflects a transient terrestrial influence. Visible

plant debris correspond to correlated peaks in Ti/Ca, C_{Tot}, N and bSi, along with lower $\delta^{13}C_{Tot}$ and stable $\delta^{15}N$ (**Fig. 3**; **Fig. S4**). Elevated bSi and $\delta^{13}C_{Tot}$ values suggest C_4 *Poacea* (*e.g.,* crop) input, as they are phytolith rich and as their $\delta^{13}C_{Tot}$ (~ -12‰) is opposed to typical C_3 plants or marine signatures (-25‰ and ~-20‰, respectively) (Descolas-Gros, 1985; Tieszen *et al.,* 1989; Cary *et al*., 2005; Katz, 2015). This localized signal, unobserved in IS02 core, highlights spatial deposition variability within the Aulne estuary. Interval "IC" features $CaCO_3$ apexes in both cores, attributed to *in-situ* production by the proliferation of *Crepidula fornicata* (Chauvaud *et al*., 2000) (**Fig. 3**). Concurrently elevated Mn and Mg align with carbonate co-precipitation (Zeller & Wray, 1956). In contrast to "IA", "IC" does not distort other proxies, implying minimal impacts on productivity dynamics and on proxy records.

Post-1946, and most notably since the 1970s, both cores display rising TOM, C_{Tot}, N, bSi, P/Al and $\delta^{15}N$, suggesting enhanced estuarine productivity, likely driven by anthropogenic nutrient loading particularly from agriculture (**Fig. 3**). These trends align with stated post-WWII phytoplankton shifts in the Bay of Brest (**Fig. 6**) (Lambert *et al*., 2018; Siano *et al.,* 2021; Valero *et al.,* 2025). Diagenetic alteration may artificially elevate proxy values, yet its effect is considered negligible below ~15 cm in such estuarine context (Wollast & De Broeu, 1971; Van Cappellen, 1996; Canfield, 1994; Burdige *et al.,* 1998; Dunn *et al*., 2017; Guillou *et al.,* 2023). The second, sharper proxy rise observed after ~1976 in IS02 (10 cm) and ~1995 in IS04 (15 cm), may partly reflect diagenetic processes given core-specific burial conditions.

The timing in IS02 core also coincides with increased regional nutrient inputs and early eutrophication (Lambert *et al*., 2018). This is supported by heavier $\delta^{15}N$ signatures (> 6 ‰) suggesting agricultural sources such as manure or synthetic fertilizers (Savoye *et al.,* 2003; Kendall & McDonnell, 2012). Minor $\delta^{15}N$ enrichment may result from ^{14}N remineralization, yet these effects are limited under oxic, N-poor conditions and where denitrification is likely minimal (Altabet & Francois, 1994). The rise of N and bSi in IS04 core before 1996, despite consistent burial depths, likely results from coarser grain-size diluting their signals more than bulk indicators like TOM or P/Al (Zhou *et al*., 2019). This is supported by progressively increased trends in TOM and P/Al, as well as historical grain-size variations. Relationships among organic C (C_{Org}), $\delta^{13}C_{Org}$ (despite significant methodological uncertainties), N, and $\delta^{15}N$; reinforce a dual signal of elevated *in situ* production due to increasing terrestrial input (**Fig.S8**; **Fig.S9**; **Fig.S10**; **Fig. S11**; **Fig. S12**; **Fig. S13**). These patterns suggest that, despite some diagenetic and grain-size biases, IS02 and IS04 cores biogenic proxies effectively track productivity dynamics in the Aulne estuary. This environment would hence have undergone strong anthropogenic perturbations: initial suppression of the productivity due to TME pollution from galena mining (uncertain chronological placement), gradual

recovery until WWII, and a pronounced post-WWII rise driven by agricultural loading.

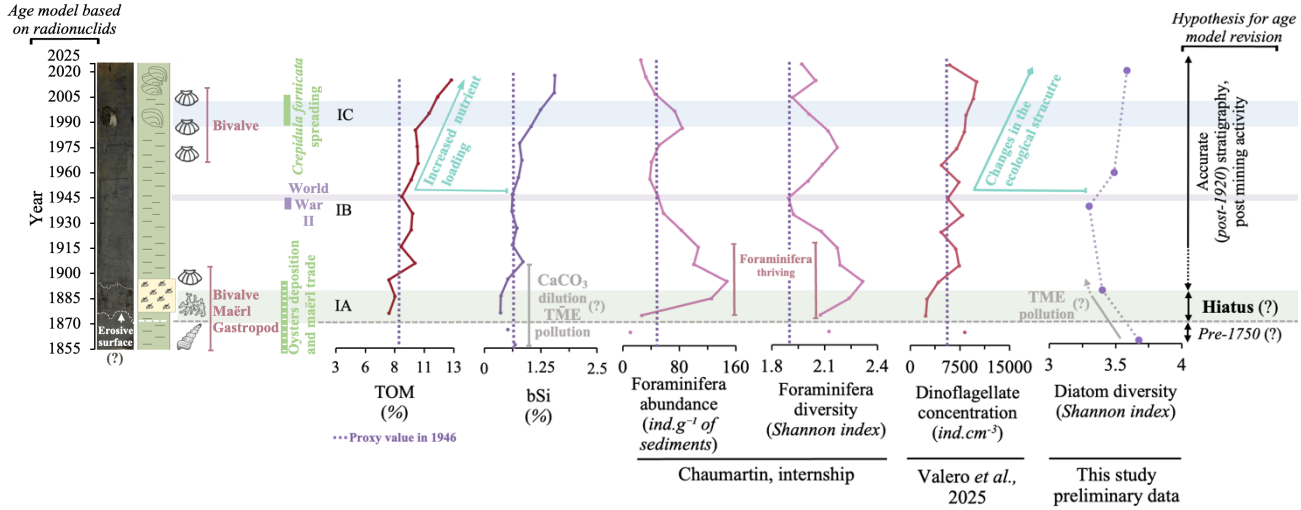

Figure 6. PACTE-AL-IS02 core integrated summary of the proxies for biogenic productivity, highlighting key sedimentological features and potential environmental drivers.

6. Conclusion

This study reconstructs 160 years of environmental variability in the Aulne estuary (Bay of Brest, NW France), focusing on the repercussion of historical mining activities and modern agricultural practices on productivity dynamics. Sedimentological and geochemical analyses from two sediment cores (PACTE-AL-IS02 and IS04 cores) reveal consistent patterns, suggesting homogenous estuarine forcing. A pronounced increase in Pb, Cd, Zn, Ag, Sb, and Cu between ~1876-1886, along with the adoption of the Poullaouen-Huelgoat mining complex Pb isotopic composition and decreasing concentrations of biogenic proxies, suggests a significant contamination event associated with the mining complex. The presence of a carbonate bed, either linked to anthropogenic marine activities, storm-related events or natural thriving, may yet have induced a sedimentological hiatus and a mis-alignment with historical mining activities. The subsequent decline in TMEs enrichment coincides with a relative increase in productivity, further amplified post-WWII by intensified agriculture. Since the 1970's, the widespread use of fertilizers may have magnified this trend, although proxy signals are still assumed to be affected by diagenetic dissolutions. The productivity of the Aulne estuary nevertheless did not seem to be significatively impacted by the rate of terrestrial inputs or by redox conditions, reinforcing the relative bio-geochemical influences of TMEs and nutrient loadings.

The Aulne estuary is hence considered to be a major vector of anthropogenic pressures, introducing historical metal contaminants and modern nutrient inputs. Future work should focus on chronological uncertainties (*e.g.*, via gastropod shell ^{14}C dating), and explore the influence of macro-carbonate layers on trace metal enrichment to refine the reconstruction of the land-sea continuum influences on the Bay of Brest over the last two centuries.

7. References

Algeo, T. J., & Liu, J. (2020). A re-assessment of elemental proxies for paleoredox analysis. Chem. Geol., 540, 119549.

Altabet, M. A., & Francois, R. (1994). Sedimentary nitrogen isotopic ratio as a recorder for surface ocean nitrate utilization. Global biogeochemical cycles, 8(1), 103-116.

Aminot, A., & Kérouel, R. (2007). Dosage automatique des nutriments dans les eaux marines: méthodes en flux continu. Editions Quae.

Anju, M., & Banerjee, D. K. (2011). Associations of cadmium, zinc, and lead in soils from a lead and zinc mining area as studied by single and sequential extractions. Environmental monitoring and assessment, 176, 67-85.

Bahr, A., Lamy, F., Arz, H., Kuhlmann, H., & Wefer, G. (2005). Late glacial to Holocene climate and sedimentation history in the NW Black Sea. Marine Geology, 214(4), 309-322.

Barrat, J. A., Zanda, B., Moynier, F., Bollinger, C., Liorzou, C., & Bayon, G. (2012). Geochemistry of CI chondrites: Major and trace elements, and Cu and Zn isotopes. Geochim. Cosmochim. Acta, 83, 79-92.

Bergamaschi, B. A., Tsamakis, E., Keil, R. G., Eglinton, T. I., Montluçon, D. B., & Hedges, J. I. (1997). The effect of grain size and surface area on organic matter, lignin and carbohydrate concentration, and molecular compositions in Peru Margin sediments. Geochimica et Cosmochimica Acta, 61(6), 1247-1260.

Birch, G. F., Gunns, T. J., & Olmos, M. (2015). Sediment-bound metals as indicators of anthropogenic change in estuarine environments. Marine pollution bulletin, 101(1), 243-257.

Blott, S. J., & Pye, K. (2001). GRADISTAT: a grain size distribution and statistics package for the analysis of unconsolidated sediments. Earth surface processes and Landforms, 26(11), 1237-1248.

Bosseboeuf, L. (2024). Jusqu'au bout? L'effondrement des ressources marines de la rade de Brest: exploitation, gestion et répétitions (XVIIIe-fin XXe siècles) (Doctoral dissertation, Université de Bretagne occidentale-Brest).

Briant, N., Waeles, M., Grouhel-Pellouin, A., Boulben, S., Lebrun, L., Akcha, F., & Sussarellu, R. (2022). Rapport d'activités projet COMENRADE : Contamination métallique de la rade de Brest et impact sur les bivalves d'intérêt conchylicole. Ifremer.

Burdige, D. J., & Zheng, S. (1998). The biogeochemical cycling of dissolved organic nitrogen in estuarine sediments. Limnology and Oceanography, 43(8), 1796-1813.

Calvert, S. E., & Pedersen, T. F. (1992). Organic carbon accumulation and preservation in marine sediments: how important is anoxia. Productivity, accumulation and preservation of organic matter in recent and ancient sediments, 231-263.

Canfield, D. E. (1994). Factors influencing organic carbon preservation in marine sediments. Chem. Geol., 114(3-4), 315-329.

Cary, L., Alexandre, A., Meunier, J. D., Boeglin, J. L., & Braun, J. J. (2005). Contribution of phytoliths to the suspended load of biogenic silica in the Nyong basin rivers (Cameroon). Biogeochemistry, 74, 101-114.

Chapelle, A., Le Gac, M., Labry, C., Siano, R., Quere, J., Caradec, F., ... & Gouriou, J. (2015). The Bay of Brest (France), a new risky site for toxic Alexandrium minutum blooms and PSP shellfish contamination. Harmful algae news, 51, 4-5.

Chapman, P. M., & Anderson, J. (2005). A decision-making framework for sediment contamination. Integrated environmental assessment and management, 1(3), 163-173.

Charles, C., Barrat, J. A., & Pelleter, E. (2021). Trace element determinations in Fe–Mn oxides by high resolution ICP-MS after Tm addition. Talanta, 233, 122446.

Chaumartin, A. (2025). Study of benthic foraminiferal communities over the past centuries in the Bay of Brest: natural vs. anthropogenic drivers? (Master's thesis). Université de Lille, Lille, France.

Chauris, L., & Marcoux, E. (1994). Metallogeny of the Armorican massif. Pre-Mesozoic geology in France and related areas, 243-264.

Chauvaud, L., Jean, F., Ragueneau, O., & Thouzeau, G. (2000). Long-term variation of the Bay of Brest ecosystem: benthic-pelagic coupling revisited. Marine Ecology Progress Series, 200, 35-48.

Chiffoleau, J.-F. (2017). La contamination chimique sur le littoral Loire-Bretagne: Résultats de 35 années de suivi du Réseau d'Observation de la Contamination Chimique (Ref. RST.RBE-BE/2017.02). Ifremer.

Costanza, R., d'Arge, R., De Groot, R., Farber, S., Grasso, M., Hannon, B., ... & Van Den Belt, M. (1997). The value of the world's ecosystem services and natural capital. nature, 387(6630), 253-260.

Cotten, J., Le Dez, A., Bau, M., Caroff, M., Maury, R. C., Dulski, P., ... & Brousse, R. (1995). Origin of anomalous rare-earth element and yttrium enrichments in subaerially exposed basalts: evidence from French Polynesia. Chemical Geology, 119(1-4), 115-138.

Dan, S. F., Li, S., Yang, B., Cui, D., Ning, Z., Huang, H., ... & Yang, J. (2021). Influence of sedimentary organic matter sources on the distribution characteristics and preservation status of organic carbon, nitrogen, phosphorus, and biogenic silica in the Daya Bay, northern South China Sea. Sci. Total Environ, 783, 146899.

Daumas, V. (2023). Les mines de plomb argentifère de Huelgoat-Poullaouen: une porte d'entrée à la technique industrielle (XVIIIe-XIXe siècles). Carhaix et le Poher. Langues de Bretagne. Actes du congrès de Carhaix. Mémoires de la Société d'Histoire et d'Archéologie de Bretagne, 101, p-169.

DeMaster, D. J. (1981). The supply and accumulation of silica in the marine environment. Geochimica et Cosmochimica acta, 45(10), 1715-1732.

Descolas-Gros, C., & Fontugne, M. R. (1985). Carbon fixation in marine phytoplankton: carboxylase activities and stable carbon-isotope ratios; physiological and paleoclimatological aspects. Mar. Bio., 87(1), 1-6.

Dunn, R. J., Waltham, N. J., Teasdale, P. R., Robertson, D., & Welsh, D. T. (2017). Short-term nitrogen and phosphorus release during the disturbance of surface sediments: A case study in an urbanised estuarine system (Gold Coast Broadwater, Australia). Journal of Marine Science and Engineering, 5(2), 16.

Elbaz-Poulichet, F., Holliger, P., Martin, J. M., & Petit, D. (1986). Stable lead isotopes ratios in major French rivers and estuaries. Science of the Total Environment, 54, 61-76.

Flatrès, P. (1963). La deuxième" Révolution agricole" en Finistère. Études rurales, (8), 5-55.

Frémion, F., Bordas, F., Mourier, B., Lenain, J. F., Kestens, T., & Courtin-Nomade, A. (2016). Influence of dams on sediment continuity: A study case of a natural metallic contamination. Sci. Total Environ., 547, 282-294.

Frontalini, F., & Coccioni, R. (2008). Benthic foraminifera for heavy metal pollution monitoring: a case study from the central Adriatic Sea coast of Italy. Estuarine, Coastal and Shelf Science, 76(2), 404-417.

Gale, N. H. (1996). A new method for extracting and purifying lead from difficult matrices for isotopic analysis. Analytica Chimica Acta, 332(1), 15-21.

Goslin J., Briant N., Scidt S., Waeles M., Madec L., Ehrhold A., Jorry S., Jouet G., Leroy P. (in prep.) - Legacy heavy metal pollution from ancient argenteous lead mines in sedimentary banks of the Aulne river, (Brittany, France)

Gourlez, E., Béline, F., Dourmad, J. Y., Monteiro, A., & De Quelen, F. (2022). Rôle et impact environnemental du cuivre et du zinc en élevage porcin: de l'alimentation au retour au sol des effluents:(Full text available in English). INRAE Productions Animales, 35(2), 91-108.

Grall, J., & Hall-Spencer, J. M. (2003). Problems facing maerl conservation in Brittany. Aquatic Conservation-Marine and Freshwater Ecosystems, 13, S55.

Guillou, N., Chapalain, G., & Petton, S. (2023). Predicting sea surface salinity in a tidal estuary with machine learning. Oceanologia, 65(2), 318-332.

Guo, T., Lou, C., Zhai, W., Tang, X., Hashmi, M. Z., Murtaza, R., ... & Xu, J. (2018). Increased occurrence of heavy metals, antibiotics and resistance genes in surface soil after long-term application of manure. Science of the Total Environment, 635, 995-1003.

Ip, C. C., Li, X. D., Zhang, G., Wai, O. W., & Li, Y. S. (2007). Trace metal distribution in sediments of the Pearl River Estuary and the surrounding coastal area, South China. Environ. Pollut., 147(2), 311-323.

Ishfaq, A. M., Pattan, J. N., Matta, V. M., & Banakar, V. K. (2013). Variation of paleo-productivity and terrigenous input in the eastern Arabian Sea during the past 100 ka. Journal of the Geological Society of India, 81, 647-654.

IUPAC. Compendium of Chemical Terminology, 2nd ed. (the "Gold Book"). Compiled by A. D. McNaught and A. Wilkinson. Blackwell Scientific Publications, Oxford (1997).

Jensen, K., Sloth, N. P., Risgaard-Petersen, N., Rysgaard, S., & Revsbech, N. P. (1994). Estimation of nitrification and denitrification from microprofiles of oxygen and nitrate in model sediment systems. Applied and Environmental Microbiology, 60(6), 2094-2100.

Jones, L. H. P., & Jarvis, S. C. (1981). The fate of heavy metals.

Katz, O. (2015). Silica phytoliths in angiosperms: phylogeny and early evolutionary history. New Phytologist, 208(3), 642-646.

Kendall, C., & McDonnell, J. J. (Eds.). (2012). Isotope tracers in catchment hydrology. Elsevier.

Lambert, C., Penaud, A., Vidal, M., Klouch, K., Gregoire, G., Ehrhold, A., ... & Siano, R. (2018). Human-induced river runoff overlapping natural climate variability over the last 150 years: Palynological evidence (Bay of Brest, NW France). Global and Planetary Change, 160, 109-122.

Le Goff, J., Patris, T., & Cotten, C. (2023). Rapport Contrat de rade de Brest : Diagnostic environnemental (Avec la collaboration de M. Auffret, P. Bailly du Bois, X. Bade, S. Ballu, *et al*.). Ifremer / Préfecture maritime / Région Bretagne.

Lechler, P. J., & Desilets, M. O. (1987). A review of the use of loss on ignition as a measurement of total volatiles in whole-rock analysis. Chemical Geology, 63(3-4), 341-344.
Li, X., Zhou, T., Li, Z., Wang, W., Zhou, J., Hu, P., ... & Wu, L. (2022). Legacy of contamination with metal (loid) s and their potential mobilization in soils at a carbonate-hosted lead-zinc mine area. Chemosphere, 308, 136589.
Liang, Q., Jing, H., & Gregoire, D. C. (2000). Determination of trace elements in granites by inductively coupled plasma mass spectrometry. Talanta, 51(3), 507-513.
Liu, S., Liu, Y., Yang, G., Qiao, S., Li, C., Zhu, Z., & Shi, X. (2012). Distribution of major and trace elements in surface sediments of Hangzhou Bay in China. Acta Oceanologica Sinica, 31, 89-100.
Loring, D. H. (1991). Normalization of heavy-metal data from estuarine and coastal sediments. ICES Journal of Marine Science, 48(1), 101-115.
Magalhães, C., Costa, J., Teixeira, C., & Bordalo, A. A. (2007). Impact of trace metals on denitrification in estuarine sediments of the Douro River estuary, Portugal. Marine Chemistry, 107(3), 332-341.
Meyers, P. A. (1994). Preservation of elemental and isotopic source identification of sedimentary organic matter. Chemical geology, 114(3-4), 289-302.
Morford, J. L., & Emerson, S. (1999). The geochemistry of redox sensitive trace metals in sediments. Geochimica et Cosmochimica Acta, 63(11-12), 1735-1750.
Murray, R. W., Miller, D. J., & Kryc, K. A. (2000). Analysis of major and trace elements in rocks, sediments, and interstitial waters by inductively coupled plasma–atomic emission spectrometry (ICP-AES).
Nasri, K., Gregoire, G., Murat, A., & Fiallo, M. (2021). Unlikely lead-bearing phases in river and estuary sediments near an ancient mine (Huelgoat, Brittany, France). Environmental Science and Pollution Research, 28(7), 8128-8139.
Negrel, P. (1997). Multi-element chemistry of Loire estuary sediments: anthropogenic *vs*. natural sources. Estuarine, Coastal and Shelf Science, 44(4), 395-410.
Orton, G. J., & Reading, H. G. (1993). Variability of deltaic processes in terms of sediment supply, with particular emphasis on grain size. Sedimentology, 40(3), 475-512.
Pan, K., & Wang, W. X. (2012). Trace metal contamination in estuarine and coastal environments in China. Science of the total environment, 421, 3-16.
Pascaud, G., Boussen, S., Soubrand, M., Joussein, E., Fondaneche, P., Abdeljaouad, S., & Bril, H. (2015). Particulate transport and risk assessment of Cd, Pb and Zn in a Wadi contaminated by runoff from mining wastes in a carbonated semi-arid context. Journal of Geochemical Exploration, 152, 27-36.
Pettijohn, F. J., Potter, P. E., & Siever, R. (2012). Sand and sandstone. Springer Science & Business Media
Pommepuy, M. (1977). SAUM de la rade de Brest. Etude courantologique. Rapport préliminaire.
Ragueneau, O., Raimonet, M., Maze, C., Coston-Guarini, J., Chauvaud, L., Danto, A., ... & Thouzeau, G. (2018). The impossible sustainability of the Bay of Brest? Fifty years of ecosystem changes, interdisciplinary knowledge construction and key questions at the science-policy-community interface. Frontiers in Marine Science, 5, 124.
Raimonet, M., Andrieux-Loyer, F., Ragueneau, O., Michaud, E., Kerouel, R., Philippon, X., ... & Mémery, L. (2013). Strong gradient of benthic biogeochemical processes along a macrotidal temperate estuary: focus on P and Si cycles. Biogeochemistry, 115, 399-417.
Raimonet, M., Ragueneau, O., Soetaert, K., Khalil, K., Leynaert, A., Michaud, E., ... & Memery, L. (2023). Benthic contribution to seasonal silica budgets in two macrotidal estuaries in North-Western France. Frontiers in Marine Science, 10, 1269142.
Recensement Agricole (2010). Ministère de l'Agriculture, de l'Agroalimentaire et de la Forêt. Agreste 2010
Reynolds, F. M. (1948). The occurrence of vanadium, chromium, and other unusual elements in certain coals. Journal of the Society of Chemical Industry, 67(9), 341-345.
Richir, J., & Gobert, S. (2016). Trace elements in marine environments: occurrence, threats and monitoring with special focus on the Costal Mediterranean. Journal of environmental and analytical toxicology, 6(1).
Savoye, N., Aminot, A., Tréguer, P., Fontugne, M., Naulet, N., & Kerouel, R. (2003). Dynamics of particulate organic matter $\delta^{15}N$ and $\delta^{13}C$ during spring phytoplankton blooms in a macrotidal ecosystem (Bay of Seine, France). Marine ecology progress series, 255, 27-41.
Sedláček, J., Bábek, O., & Grygar, T. M. (2013). Trends and evolution of contamination in a well-dated water reservoir sedimentary archive: the Brno Dam, Moravia, Czech Republic. Environ. Earth Sci., 69, 2581-2593.
Serpaud, B., Al-Shukry, R., Casteignau, M., & Matejka, G. (1994). Adsorption des métaux lourds (Cu, Zn, Cd et Pb) par les sédiments superficiels d'un cours d'eau: rôle du pH, de la température et de la composition du sédiment. Revue des sciences de l'eau, 7(4), 343-365.

Sholkovitz, E. R., & Price, N. (1980). The major-element chemistry of suspended matter in the Amazon Estuary. Geochimica et Cosmochimica Acta, 44(2), 163-171.
Siano, R., Lassudrie, M., Cuzin, P., Briant, N., Loizeau, V., Schmidt, S., ... & Penaud, A. (2021). Sediment archives reveal irreversible shifts in plankton communities after World War II and agricultural pollution. Current Biology, 31(12), 2682-2689.
Siebert, V., Fröhlich, L., Thébault, J., Schöne, B. R., Delebecq, G., Picheral, M., ... & Moriceau, B. (2024). Dynamics of molybdenum and barium in the Bay of Brest (France) explained by phytoplankton community structure and aggregation events. Estuarine, Coastal and Shelf Science, 303, 108783.
Stone, M., Mulamoottil, G., & Logan, L. (1995). Grain size distribution effects on phosphate sorption by fluvial sediment: implications for modelling sediment-phosphate transport. Hydrol. Sci. J., 40(1), 67-81.
Sun, R., Gao, Y., Xu, J., Yang, Y., & Zhang, Y. (2021). Contamination Features and Source Apportionment of Heavy Metals in the River Sediments around a Lead-Zinc Mine: A Case Study in Danzhai, Guizhou, China. Journal of Chemistry, 2021(1), 9946026.
Šurija, B., & Branica, M. (1995). Distribution of Cd, Pb, Cu and Zn in carbonate sediments from the Krka river estuary obtained by sequential extraction. Science of the total environment, 170(1-2), 101-118.
Sutherland, R. A. (2000). Bed sediment-associated trace metals in an urban stream, Oahu, Hawaii. Environmental geology, 39, 611-627
Thienpont, J. R., Korosi, J. B., Hargan, K. E., Williams, T., Eickmeyer, D. C., Kimpe, L. E., ... & Blais, J. M. (2016). Multi-trophic level response to extreme metal contamination from gold mining in a subarctic lake. Proceedings of the Royal Society B: Biological Sciences, 283(1836), 20161125.
Tieszen, Larry L. et Boutton, Thomas W. Stable carbon isotopes in terrestrial ecosystem research. In : Stable isotopes in ecological research. New York, NY: Springer New York, 1989. p. 167-195.
Tilman, D. (1982). Resource competition and community structure (No. 17). Princeton university press.
Tribovillard, N., Algeo, T. J., Lyons, T., & Riboulleau, A. (2006). Trace metals as paleoredox and paleoproductivity proxies: an update. Chemical geology, 232(1-2), 12-32.
Tribovillard, N., Du Châtelet, E. A., Gay, A., Barbecot, F., Sansjofre, P., & Potdevin, J. L. (2013). Geochemistry of cold seepage-impacted sediments: per-ascensum or per-descensum trace metal enrichment?. Chemical Geology, 340, 1-12.
Turner, R. K. (2015). "Introduction," in Coastal Zones Ecosystem Services. Studies in Ecological Economics, Vol. 9, eds R. K. Turner and M. Schaafsma (Cham: Springer), 1–7.
Valero, C., Penaud, A., Vidal, M., Schmidt, S., Guérin, T., Dessandier, P. A., Goubert, E., Glémarec, E., Brigode, P., Bosseboeuf, L., Paulet, Y. M., Sutton, J., Niass, N. C., Ailliot, P., Derrien, J. M., Saguet, L., Liorzou, C., Revillon, S., Lambert, C., & R. (2025). Past trajectory of a northwest Europe socio-ecosystem at the land–sea interface: The case of the northern watersheds of the Bay of Brest over the last 150 years.
Van Cappellen, P. (1996). Reactive surface area control of the dissolution kinetics of biogenic silica in deep-sea sediments. Chemical Geology, 132(1-4), 125-130.
Van Vliet-Lanoë, B., Goslin, J., Hallégouët, B., Hénaff, A., Delacourt, C., Fernane, A., ... & Penaud, A. (2014). Middle-to late-Holocene storminess in Brittany (NW France): Part I–morphological impact and stratigraphical record. The Holocene, 24(4), 413-433.
White, W. M., Albarède, F., & Télouk, P. (2000). High-precision analysis of Pb isotope ratios by multi-collector ICP-MS. Chemical Geology, 167(3-4), 257-270.
Whitmore, G. P., Crook, K. A., & Johnson, D. P. (2004). Grain size control of mineralogy and geochemistry in modern river sediment, New Guinea collision, Papua New Guinea. Sediment. Geol., 171(1-4), 129-157.
Wollast, R., & De Broeu, F. (1971). Study of the behavior of dissolved silica in the estuary of the Scheldt. Geochimica et Cosmochimica Acta, 35(6), 613-620.
Yano, M., Yasukawa, K., Nakamura, K., Ikehara, M., & Kato, Y. (2020). Geochemical features of redox-sensitive trace metals in sediments under oxygen-depleted marine environments. Minerals, 10(11), 1021.
Zeller, E. J., & Wray, J. L. (1956). Factors influencing precipitation of calcium carbonate. AAPG Bulletin, 40(1), 140-152.
Zhang, Y., Song, B., & Zhou, Z. (2023). Pollution assessment and source apportionment of heavy metals in soil from lead–Zinc mining areas of south China. J. Environ. Chem. Eng., 11(2), 109320.
Zhou, P., Li, D., Zhao, L., Li, H., Ni, Z., Zhao, F., ... & Li, X. (2019). A 120-year sedimentary record and its environmental implications, in a dated marine sediment core from Daya Bay in the northeastern South China Sea. Marine Pollution Bulletin, 145, 248-253.
Zhu, G., Xiao, H., Guo, Q., Song, B., Zheng, G., Zhang, Z., ... & Okoli, C. P. (2018). Heavy metal contents and enrichment characteristics of dominant plants in wasteland of the downstream of a lead-zinc mining area in Guangxi, Southwest China. Ecotoxicology and Environmental safety, 151, 266-271.

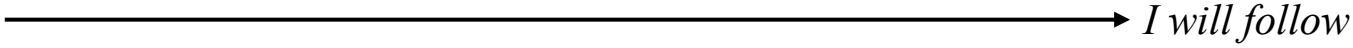
I will follow

Abstract

The Bay of Brest is a heavily stressed coastal environment, influenced by historical mining pollution from the Poullaouen-Huelgoat (P-H) complex (notably extracting galena, PbS) and ongoing agricultural inputs from the Aulne River watershed. This study reconstructs 160 years of Trace Metal Elements (TMEs) and nutrients contamination, sources, and ecological impacts using geochemical profiles from two estuarine sediment cores. TME Enrichment Factors (EFs) and isotope compositions do not align with the chronology of the P-H complex, as background values are recorded in 1857, after peak activity, while EFs rise by 1886, post-closure. The presence of a macro-carbonate bed suggests a potential sedimentological hiatus in the record of mining activities. Despite progressive decline, TME pollution remains persistent (*e.g.*, EF_{Pb} up to 5.1), indicating insufficient remediation. Post-1946, increases in the concentration of biogenic productivity proxies and terrestrial organic inputs are linked to intensified agricultural inputs, coinciding with structural ecological changes in the Bay of Brest planktonic and benthic communities, including the Aulne estuary. These findings highlight the role of the Aulne River's as a long-term vector of anthropogenic contamination.

SUPPORTING INFORMATION

160 years of environmental change in the Aulne estuary (Bay of Brest): a geochemical reconstruction of mining legacy and productivity dynamics

“Dé- ←

Table of supporting contents

List of Supporting figures

8. Supporting information

8.1. Material and methods

8.1.1. Sediment cores dating

PACTE-AL-IS02 and PACTE-AL-IS04 cores sediment dating was established on excess ^{210}Pb (^{210}Pbxs), ^{137}Cs, and ^{226}Ra radioactive isotopes depth activities at the EPOC laboratory (CNRS, University of Bordeaux). Age-depth models were provided by SCHMIDT, Sabine (**Fig. S1**)

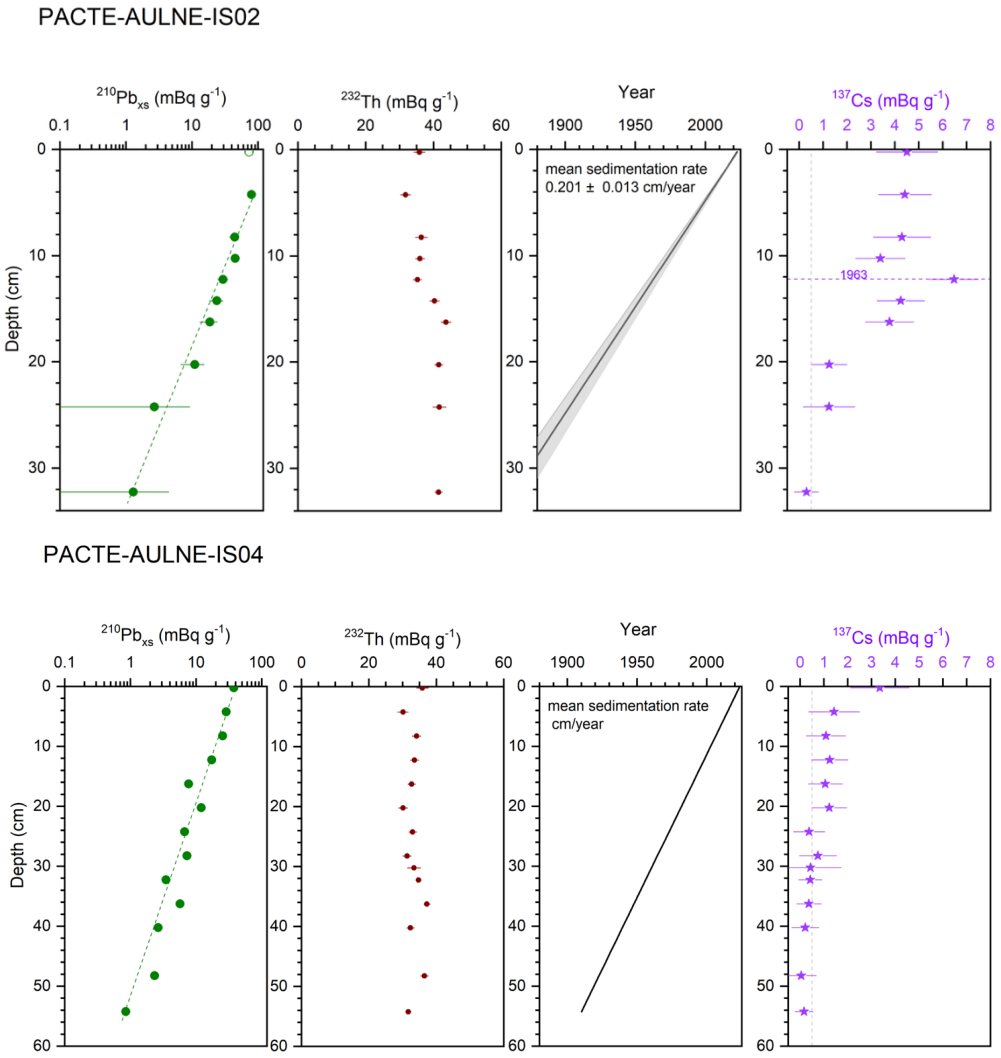

Figure S1. PACTE-AL-IS02 and PACTE-AL-IS04 cores age-depth models, based on ^{210}Pbxs, ^{232}Th and ^{37}Cs activities.

8.1.2. Geochemistry

8.1.2.a. Major and minor elements

The concentrations of major and minor oxides were measured using an Inductively Coupled Plasma-Atomic Emission Spectrometer (ICP-AES; Jobin-Yvon Ultima 2, Horiba®) at the *PSO* (**Fig. S2A**). Recoveries were expressed as the percentage of the sum of all measured oxides plus weight Loss On Ignition (LOI) relative to 100% (estimating the mass loss of sediment due to its volatility;

i.e., bound water, organic matter, sulphides, $CaCO_3$). LOI were estimated on 500 mg of sediments powders, heated using a muffle furnace to 1500°C for two hours (**Tab. S1**).

Table 1. PACTE-AL-IS02 and PACTE-AL-IS04 cores summary tab of the Loss On Ignition and oxide recovery values

PACTE-AL-IS02	**Age**	**2016**	**2006**	**1996**	**1986**	**1976**	**1966**	**1956**	**1946**	**1936**	**1926**	**1916**	**1906**	**1896**	**1886**	**1876**	**1866**	**1857**
	Loss On Ignition (%)	18.9	15.7	17.2	15.5	16.4	15.7	15.7	15.5	15.0	15.1	16.0	18.0	17.3	16.9	16.9	16.9	16.9
	Recovery (%)	*99.1*	*98.0*	*96.5*	*98.8*	*99.3*	*99.9*	*100.8*	*99.1*	*98.8*	*95.3*	*98.7*	*101.0*	*97.6*	*98.0*	*94.0*	*94.4*	*96.4*
PACTE-AL-IS04	**Age**	**2023**	**2021**	**2019**	**2015**	**2011**	**2007**	**2004**	**2000**	**1999**	**1995**	**1991**	**1987**	**1983**	**1979**	**1974**	**1970**	**1966**
	Loss On Ignition (%)	11.7	11.0	11.2	11.3	11.1	10.7	10.1	13.4	12.1	11.6	8.7	7.7	8.1	10.7	10.4	10.4	7.2
	Recovery (%)	*99.9*	*98.7*	*97.2*	*97.9*	*96.6*	*98.7*	*98.2*	*98.2*	*99.0*	*98.5*	*98.6*	*98.0*	*97.2*	*100.1*	*96.2*	*97.1*	*95.1*
	Age	**1962**	**1958**	**1954**	**1950**	**1946**	**1942**	**1938**	**1934**	**1930**	**1926**	**1922**	**1918**	**1914**				
	Loss On Ignition (%)	7.4	13.1	11.2	9.4	21.3	9.9	11.2	12.5	9.9	13.1	8.3	11.7	6.3				
	Recovery (%)	*99.0*	*98.3*	*100.6*	*97.1*	*97.9*	*97.4*	*97.4*	*99.4*	*97.6*	*98.9*	*97.5*	*99.8*	*97.2*				

The concentrations of organic C (C_{Org}, %) and its associated stable isotope ratio ($\delta^{13}C_{Org}$, ‰) were measured as described in *3.4.1.b.* with identical analytical precisions, on a batch of 5 mg decarbonated sediments powders (37% HCl; over-aggressive for accurate measures) (**Fig. S2B**). C_{Org}/N were then also derived from C_{Org} and N (measured on untreated sediments powders).

8.1.2.b. Trace elements

The concentrations of a selection of Trace Metallic Elements (i.e. Ag, Cd, Co, Cr, Cu, Hg, Mo, Ni, Pb, U, V, Sb and Zn, ppm) were measured using a High Resolution-Inductively Coupled Plasma-Mass Spectrometer (HR-ICP-MS; Element XR™, Thermo Scientific™) at the *PSO* (**Fig. S2C**). The concentrations of Rare Earth Elements (REE) were also measured and normalized to the Past Archean Australian Shale (PAAS) to highlight enrichment and depletion trends (McLennan, 2001).

8.1.2.c. Statistical analysis

Relationships between C_{Tot}/N and $\delta^{13}C_{Tot}$; C_{Tot} and $\delta^{13}C_{Tot}$; C_{Org}/N and $\delta^{13}C_{Org}$; C_{Org} and $\delta^{13}C_{Org}$; C_{Org}/N and $\delta^{13}C_{Org\text{-}IR\text{-}MS}$; C_{Org} and $\delta^{13}C_{Org}$; and N and $\delta^{15}N$, were highlighted using Hierarchical Cluster Analysis (HCA). The variability of C_{Tot}/N, C_{Org}/N and $\delta^{13}C_{Org}$ was used to identify 3 temporal clusters for each core with the *scale ()* (Min-Max scaling), *hclust()* (Ward.D2 method) and *dist()* (pairwise Euclidean distances) functions (**Fig. S3**; **Fig. S4**; **Fig. S5**; **Fig. S6**; **Fig. S7; Fig. S8**). (Murtagh & Legendre, 2014). Similarly, PCA were performed as in **3.5.,** but on 3 temporal clusters, based on the variability of D50, Al, Ti/Al, C_{Tot} and $CaCO_3$. REE/PAAS variations were also studied as temporal clusters (**Fig. S9**).

8.1.3 Diatom analysis

Ecological indexes were calculated, namely the Shannon diversity (H'; **Eq. S1**), the Pielou evenness (J; **Eq. S2**), the Margalef richness (d; **Eq. S3**) and the Simpson dominance (D; **Eq. S4**) indexes (**Eq. S5**) (**Fig. S1.C**) (Shannon, 1948; Simpson, 1949; Pielou, 1966; Margalef, 1973; Kelly *et al.,* 2001).

$$H' = -\sum_{i=1}^{S} a_i \times ln(a_i) \textbf{(S1)} \qquad J = \frac{H'}{Ln(S)} \textbf{(S2)} \qquad d = \frac{(S-1)}{Ln(N)} \textbf{(S3)} \qquad D = \frac{1}{\sum_{i=1}^{S} a_{i^2}} \textbf{(S4)}$$

Where S is the total number of taxa; i is the name of the taxon of interest; a_i its relative Abundance (RA), N is the total number of individuals.

8.2. Results figures

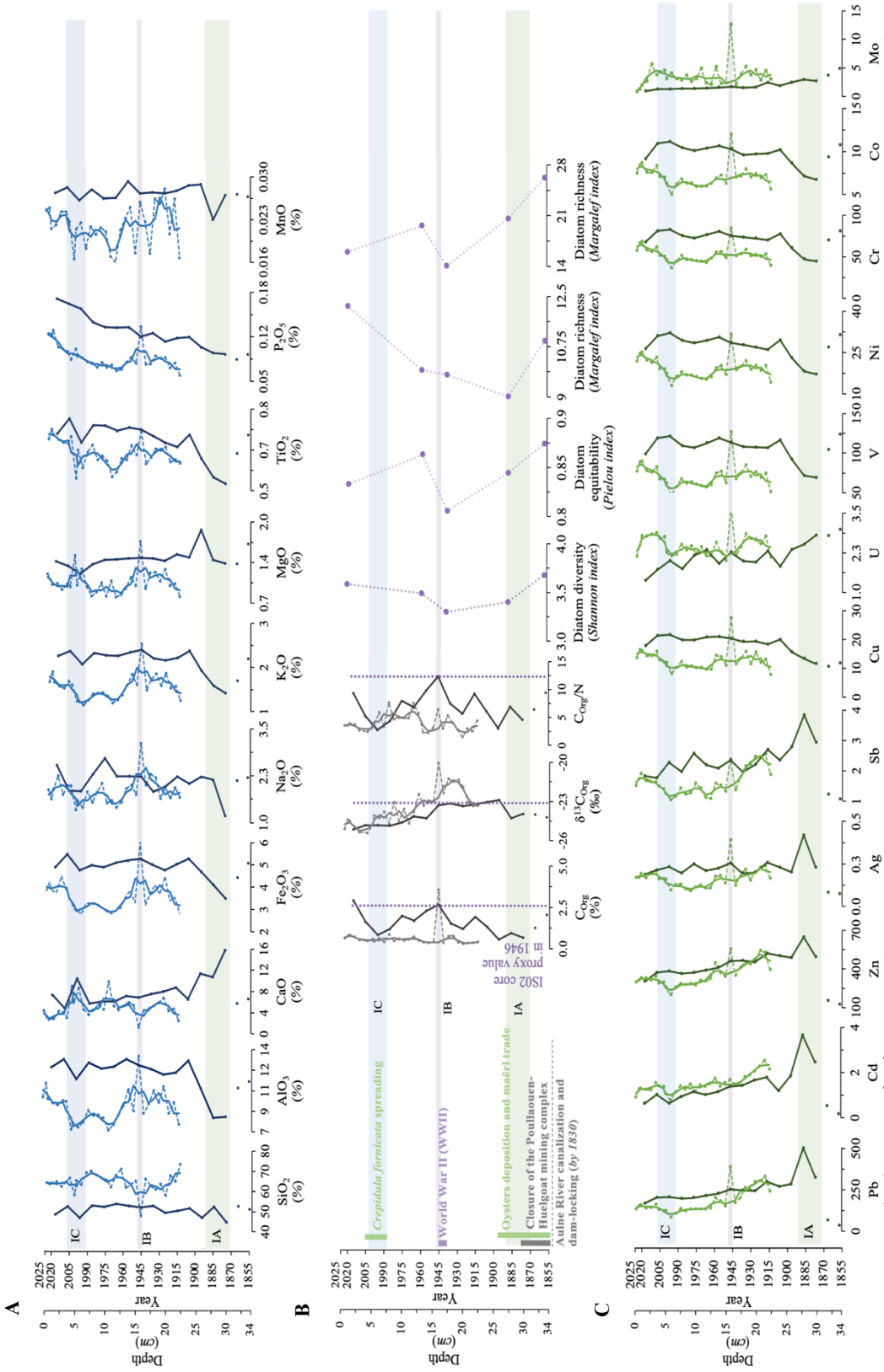

Figure S2. PACTE-AL-IS02 and PACTE-AL-IS04 cores multi-proxy data for (**A**) oxide concentrations (ICP-AES data, blue curves), (**B**) biogenic productivity (IR-MS data, grey curves; diatom counting, purple curves, featuring chronological markers of key anthropological and ecological events in the Bay of Brest and the Aulne River watershed; (**C**) Trace Metallic Elements concentrations (ICP-MS data, green curves, green curves). The two lower curves lines were not traced due to chronological uncertainties (5.1.3.b). **IA**, **IB** and **IC** stand respectively for Intervals "IA", "IB" and "IC".

PACTE-AL-IS02

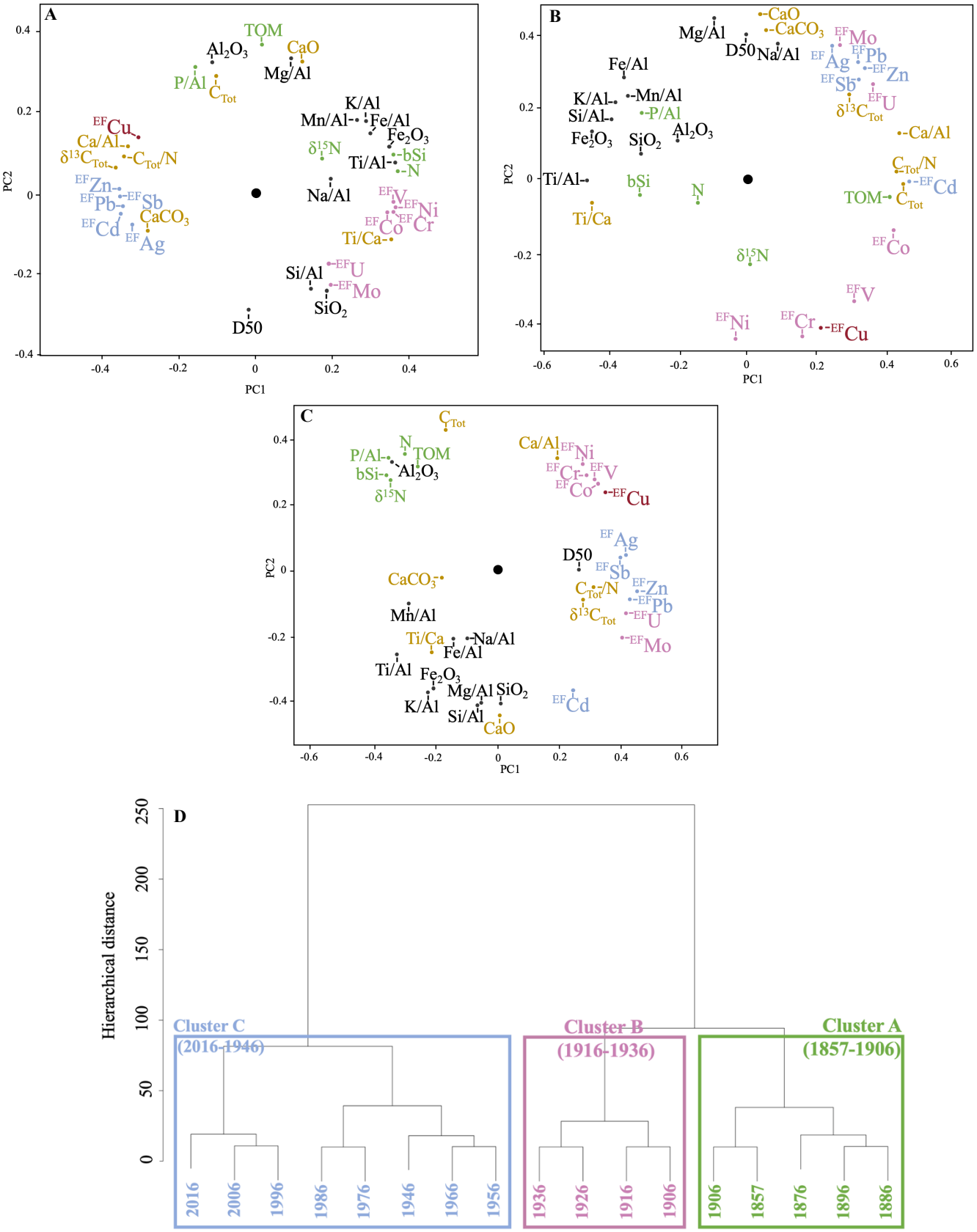

Figure S3. PACTE-AL-IS02 (**A**; **B**; **C**) Principal Components Analysis based on temporal clusters and (**D**) clustering, based on the variability of D50, %Al, Ti/Al, $\%C_{Tot}$ and $\%CaCO_3$. Analysis includes the proxies most relevant for biogenic productivity (green); assessing the pollution from the Poullaouen-Huelgoat mining complex (blue); weathering and redox conditions (pink); and proxies numerically influenced by carbonate shell banks (gold).

PACTE-AL-IS04

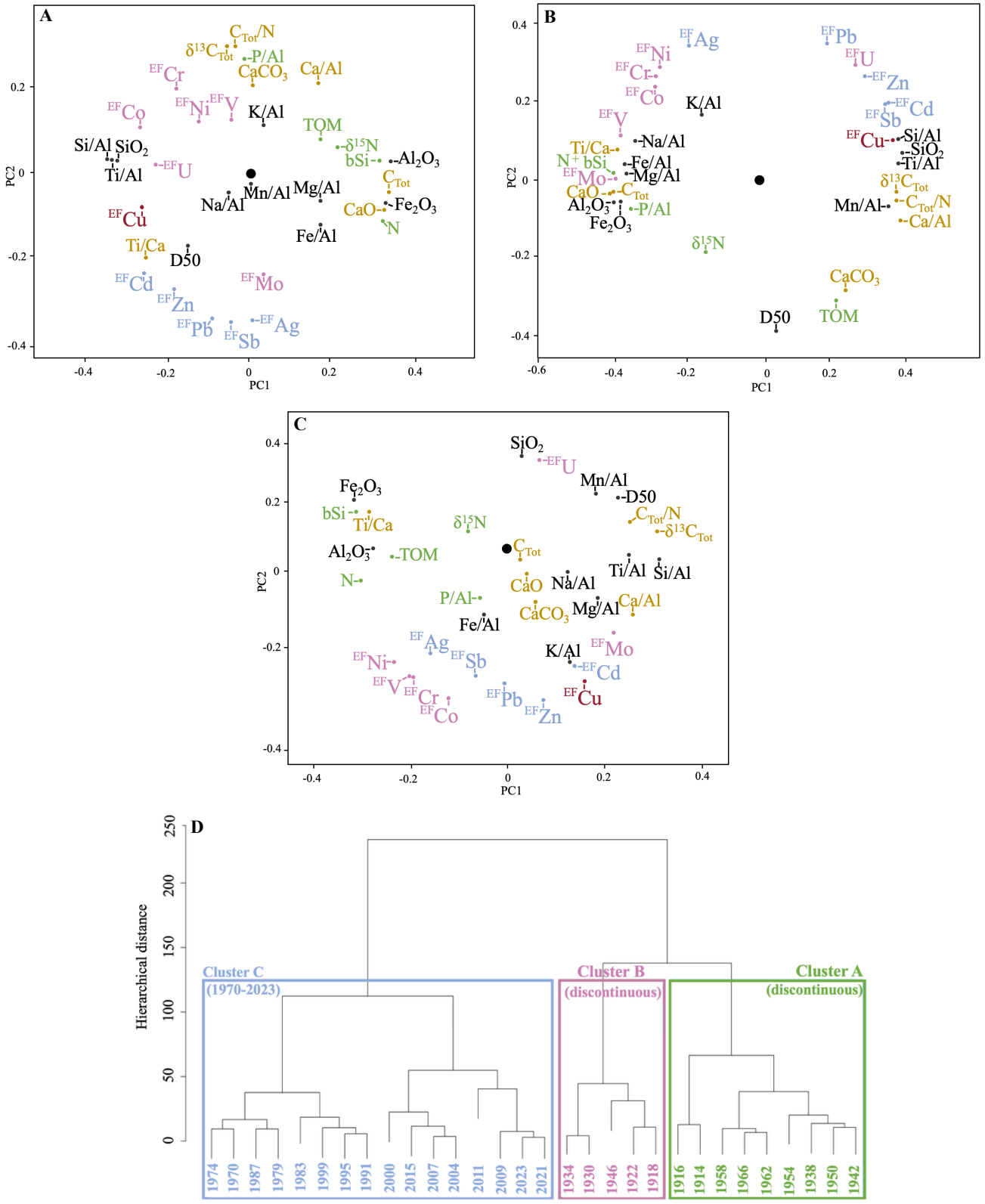

Figure S4. PACTE-AL-IS04 (**A**; **B**; **C**) Principal Components Analysis based on temporal clusters and (**D**) clustering, based on the variability of D50, %Al, Ti/Al, $\%C_{Tot}$ and $\%CaCO_3$. Analysis includes the proxies most relevant for biogenic productivity (green); assessing the pollution from the Poullaouen-Huelgoat mining complex (blue); weathering and redox conditions (pink); and proxies numerically influenced by carbonate shell banks (gold).

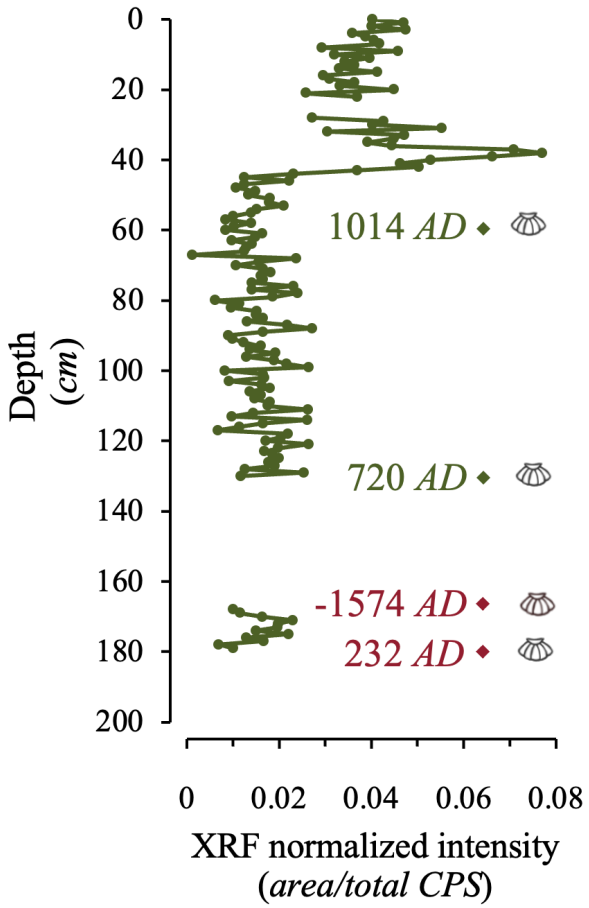

Figure S5. PACTE-AL-KS04 X-Ray Fluorescence profile for Pb. Radiocarbon (^{14}C) dates obtained from associated oyster shells are indicated for chronological references. Red dates stand for inaccurate chronologies.

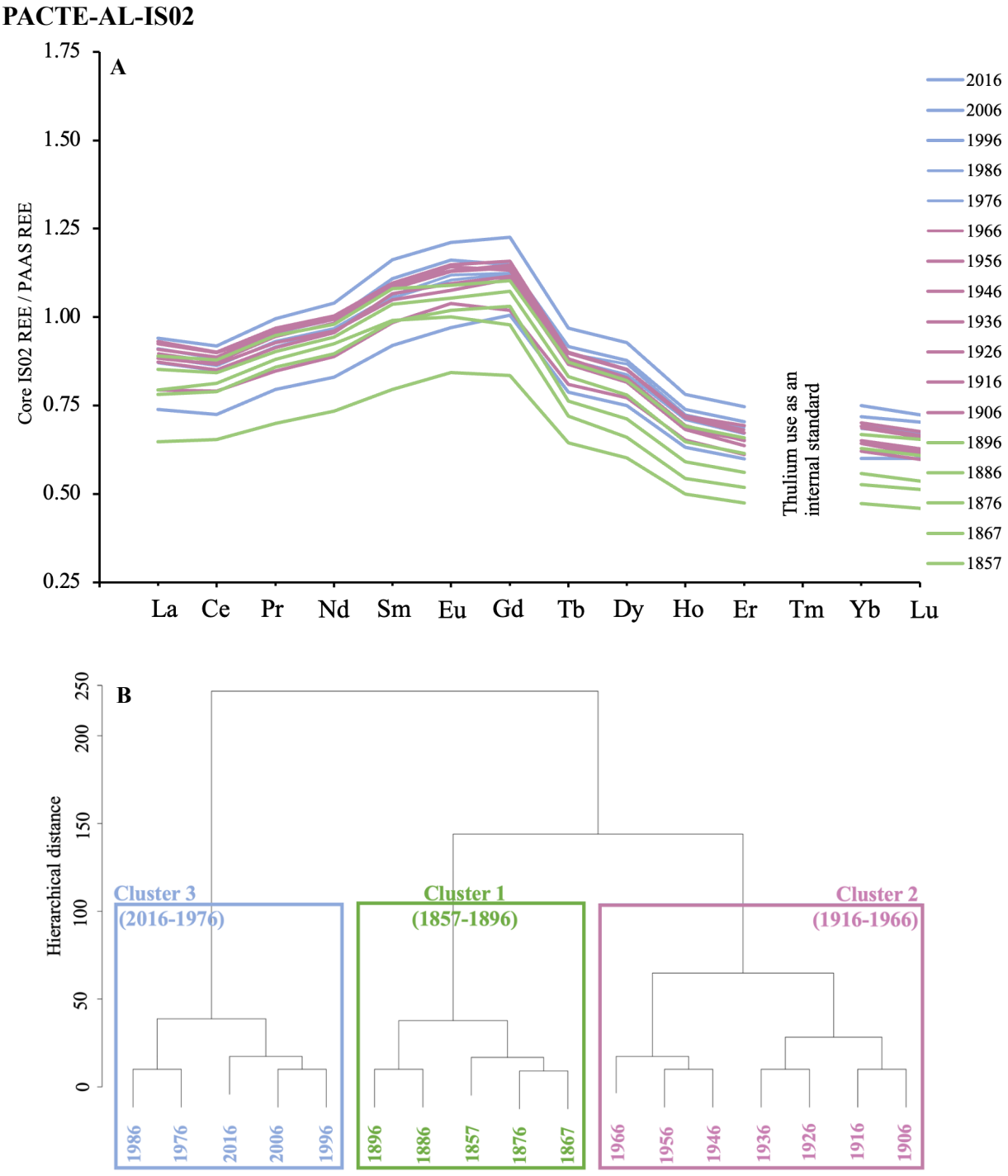

Figure S6. PACTE-AL-IS02 (**A)** REE/PAAS variations and (**B**) associated clustering.

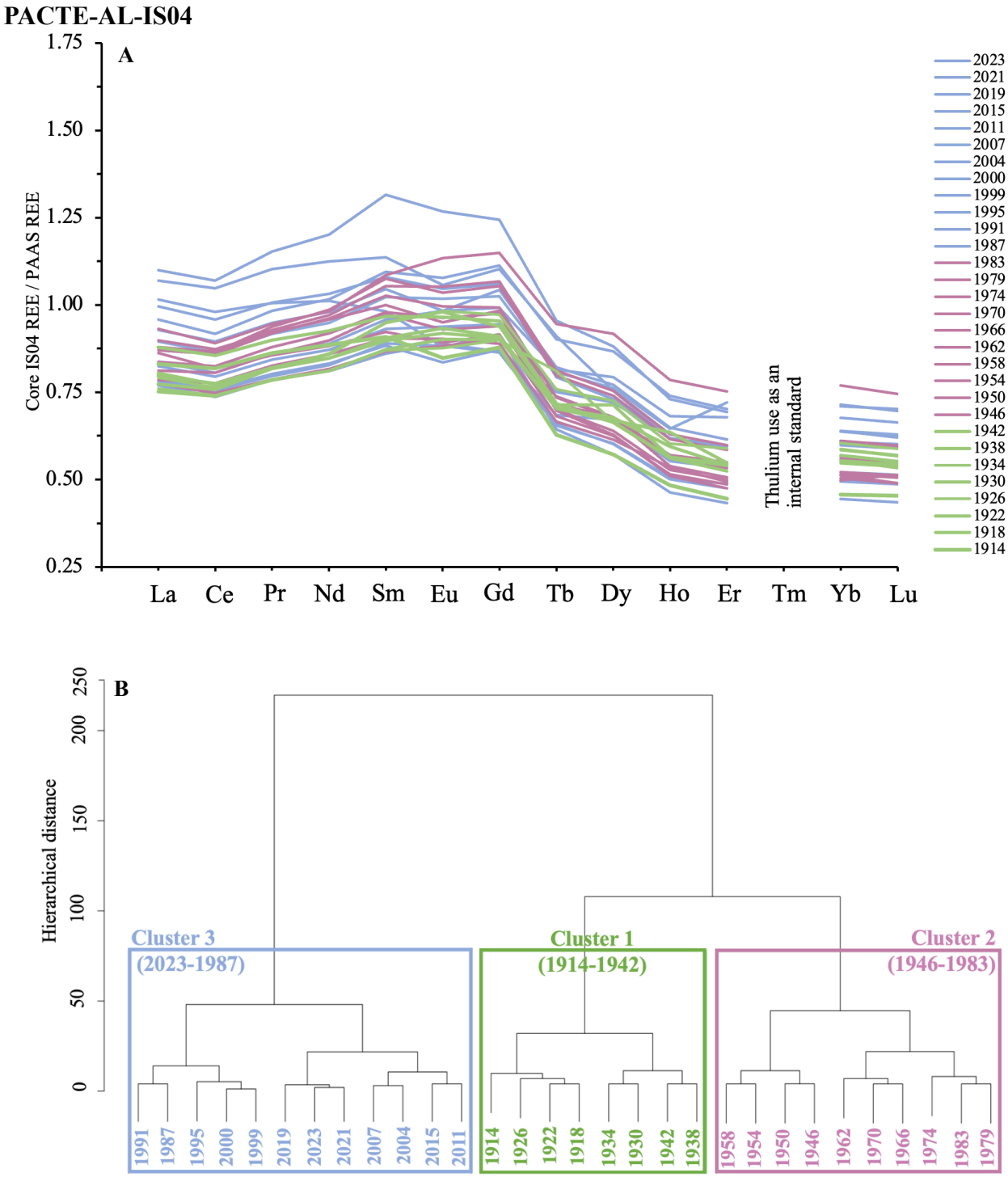

Figure S7. PACTE-AL-IS04 (**A**) REE/PAAS variations and (**B**) associated clustering.

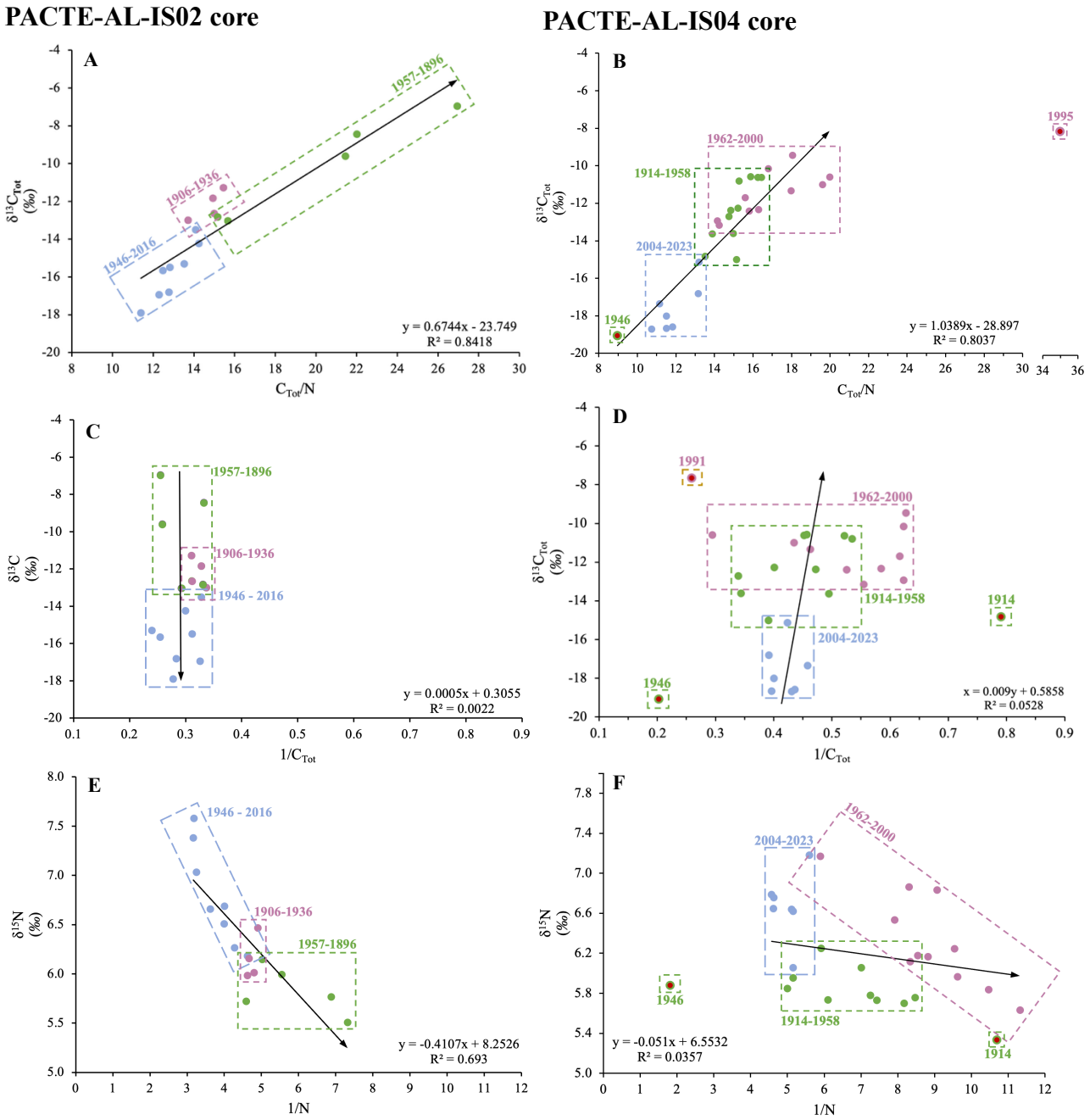

Figure S9. PACTE-AL-IS02 and PACTE-AL-IS04 cores relationships between (**A**; **B**) C_{Tot}/N and $\delta^{13}C_{Tot}$; (**C**; **D**) $\%C_{Tot}$ and $\delta^{13}C_{Tot}$; (**E**; **F**) %N and $\delta^{15}N$, based on the clustering of **Fig. S9** and **S10**.

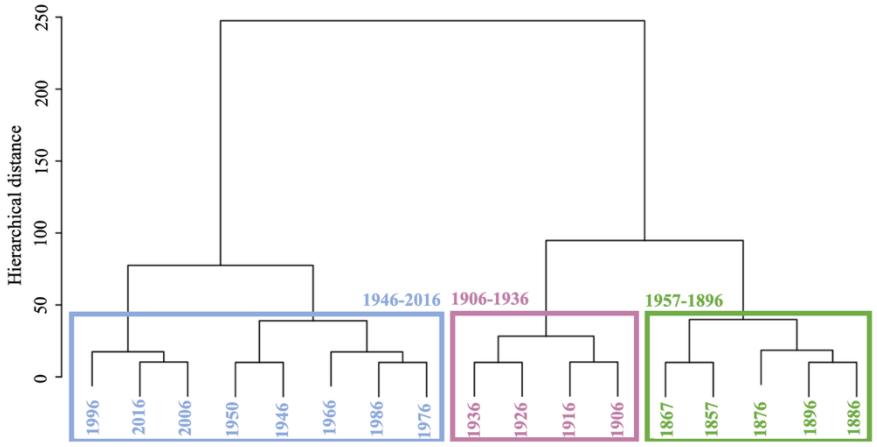

Figure S8. PACTE-AL-IS02 clustering based on the variability $\%C_{Tot}$, $\delta^{13}C_{Tot}$, %N and $\delta^{15}N$.

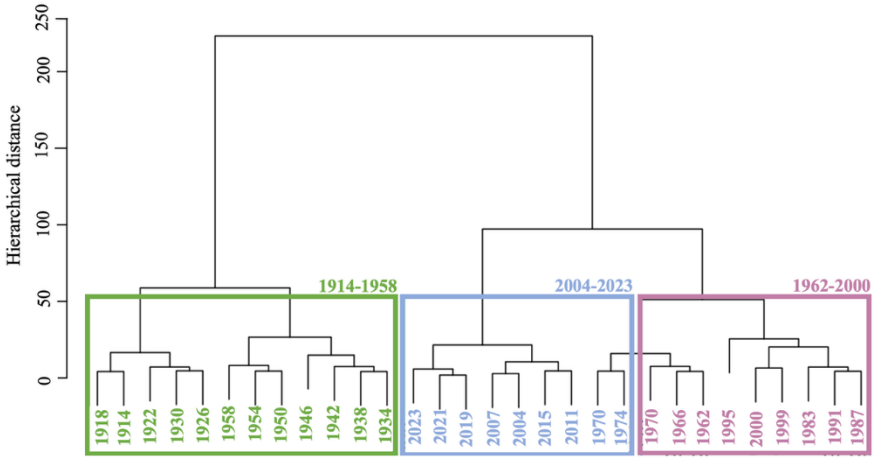

Figure S10. PACTE-AL-IS04 clustering based on the variability $\%C_{Tot}$, $\delta^{13}C_{Tot}$, %N and $\delta^{15}Nd$

PACTE-AL-IS02 core **PACTE-AL-IS04 core**

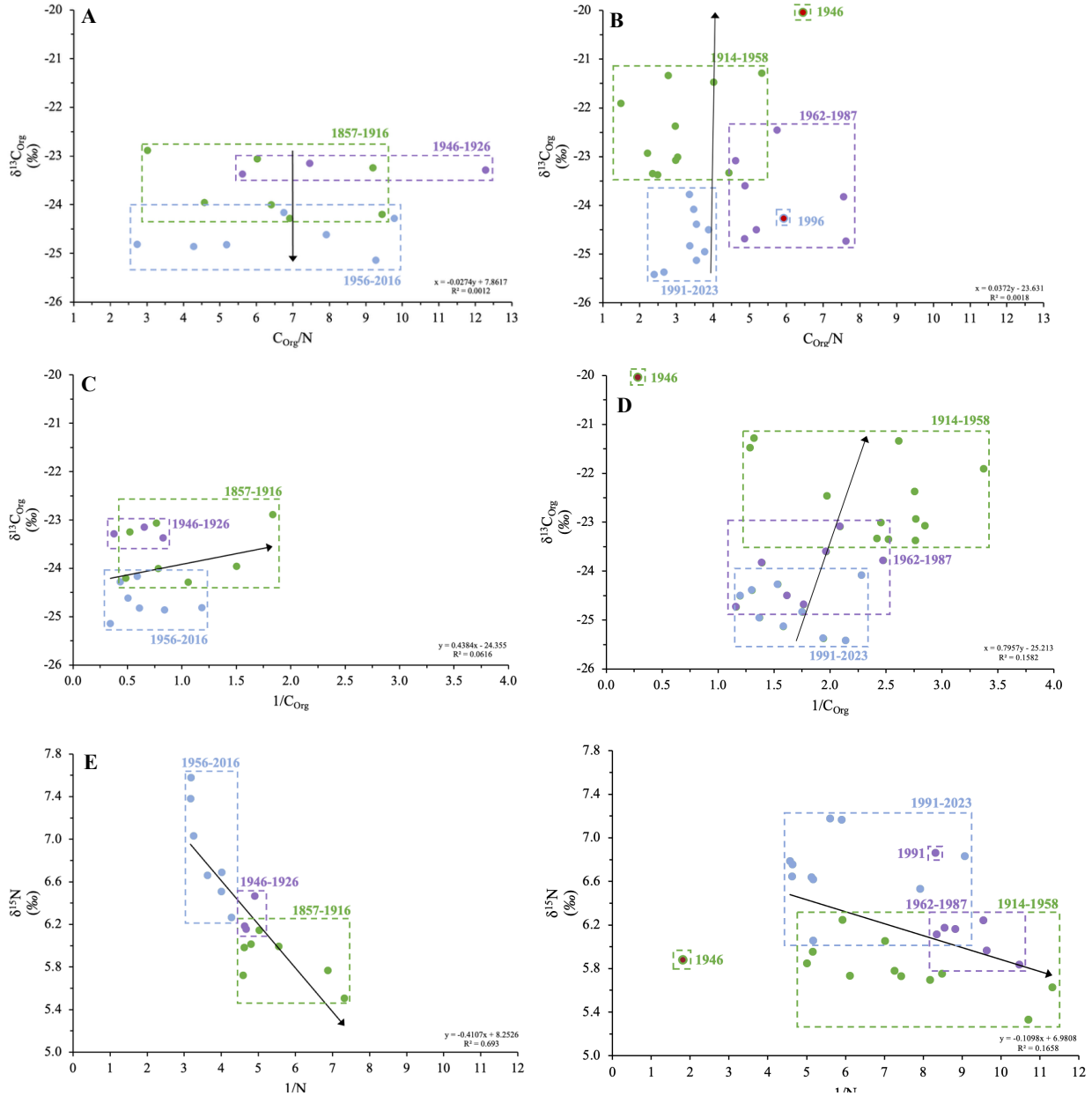

Figure S11. PACTE-AL-IS02 and PACTE-AL-IS04 cores relationships between (**A**; **B**) C_{Org}/N and $\delta^{13}C_{Org}$; (**C**; **D**) $\%C_{Org}$ and $\delta^{13}C_{Org}$; (**E**; **F**) %N and $\delta^{15}N$; based on the clustering of **Fig. S11** and **S12**.

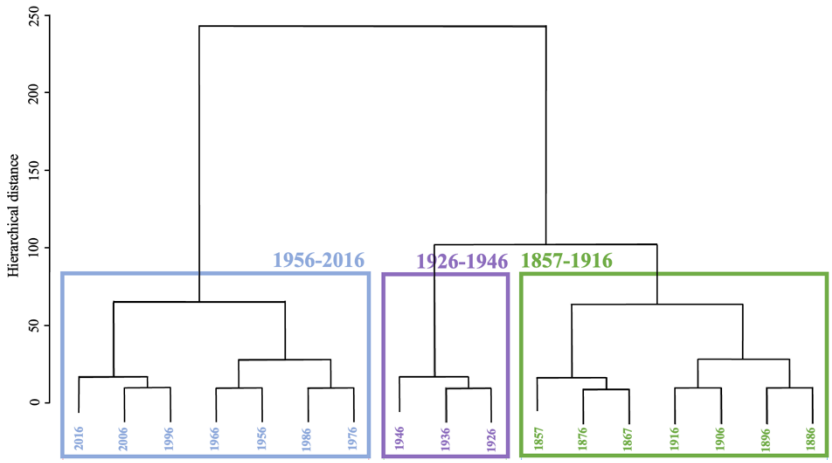

Figure 12. PACTE-AL-IS02 clustering based on the variability $\%C_{Org}$, $\delta^{13}C_{Org}$, %N and $\delta^{15}N$.

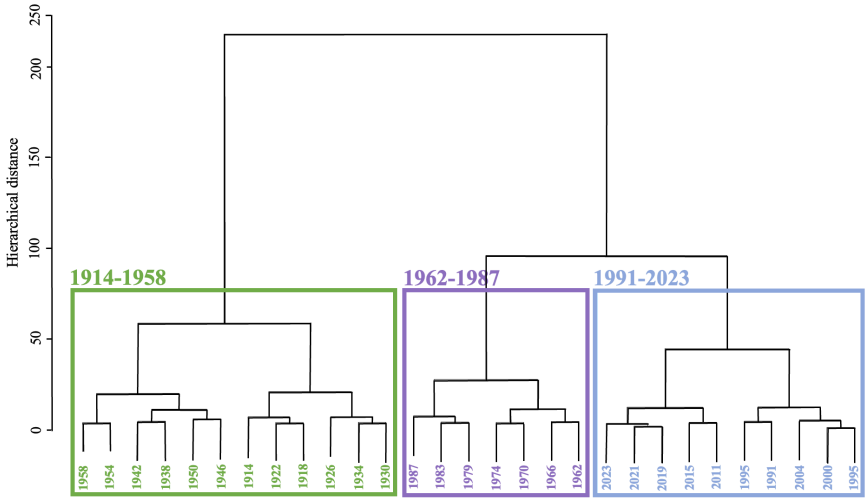

Figure S13. PACTE-AL-IS04 clustering based on the variability $\%C_{Org}$, $\delta^{13}C_{Org}$, %N and $\delta^{15}N$.

7.3. References

Crosta, X., & Koç, N. (2007). Chapter eight diatoms: From micropaleontology to isotope geochemistry. Developments in marine geology, 1, 327-369.

Crosta, X., Shukla, S. K., Ther, O., Ikehara, M., Yamane, M., & Yokoyama, Y. (2020). Last Abundant Appearance Datum of Hemidiscus karstenii driven by climate change. Mar. Micropaleontol., 157, 101861.

Heiri, O., Lotter, A. F., & Lemcke, G. (2001). Loss on ignition as a method for estimating organic and carbonate content in sediments: reproducibility and comparability of results. Journal of paleolimnology, 25, 101-110.

Kihara, Y., Tsuda, K., Ishii, C., Ishizumi, E., & Ohtsuka, T. (2015). Periphytic diatoms of Nakaikemi Wetland, an ancient peaty low moor in central Japan. Diatom, 31, 18-44.

Margalef, R. (1973). Information theory in ecology.

McLennan, S. M. (2001). Relationships between the trace element composition of sedimentary rocks and upper continental crust. Geochemistry, geophysics, geosystems, 2(4).

Murtagh, F., & Legendre, P. (2014). Ward's hierarchical agglomerative clustering method: which algorithms implement Ward's criterion?. Journal of classification, 31, 274-295.

Park, J., Khim, J. S., Ohtsuka, T., Araki, H., Witkowski, A., & Koh, C. H. (2012). Diatom assemblages on Nanaura mudflat, Ariake Sea, Japan: with reference to the biogeography of marine benthic diatoms in Northeast Asia. Botanical studies, 53(1).

Paulmier, G. (1997). Atlas des diatomophycées des côtes françaises et des aires océaniques adjacentes.

Pielou, E. C. (1966). The measurement of diversity in different types of biological collections. Journal of theoretical biology, 13, 131-144.

Shannon, C. E. (1948). A mathematical theory of communication. The Bell system technical journal, 27(3), 379-423.

Simpson, E. H. (1949). Measurement of diversity. nature, 163(4148), 688-688.

Siqueiros Beltrones, D. A., Argumedo Hernández, U., & Landa Cansigno, C. (2016). Uncommon species diversity values in epiphytic diatom assemblages of the kelp Eisenia arborea. Hidrobiológica, 26(1), 61-76.

Siqueiros Beltrones, D. A., López-Fuerte, F. O., Martínez, Y. J., & Altamirano-Cerecedo, M. D. C. (2021). A first estimate of species diversity for benthic diatom assemblages from the Revillagigedo Archipelago, México. Diversity, 13(10), 458.

———————————————————————————— *-cidément ?”*

Université de Bretagne Occidentale

iversité est une chance

ENGAGEMENT DE NON PLAGIAT

Je soussignée **GIRARDOT Margot**

Assure avoir pris connaissance de la charte anti-plagiat de l'université de Bretagne occidentale.

Je déclare être pleinement consciente que le plagiat total ou partiel de documents publiés sous différentes formes, y compris sur internet, constitue une violation des droits d'auteur ainsi qu'une fraude caractérisée.

Je m'engage à citer toutes les sources que j'ai utilisées pour rédiger ce travail.

Signature

Document à insérer en première page de tous les rapports, dossiers et mémoires.